Application of Atmospheric Pressure Atomic Layer Deposition on Long Tubular Ceramic Membranes

CIE5050-09 Additional Graduation Work

Prepared by
Mrinal Roy
(4724410)

Supervised by
Dr. Ir. Ran Shang
Dr. Ir. Bas Heijman
Dr. Ir. Ralph Lindeboom
Ir. Irene Caltran

January 2019

Department of Environmental Engineering
Faculty of Civil Engineering and Geoscience
Delft University of Technology

Summary

Recently, the use of atomic layer deposition (ALD) technique for depositing thin films of metal oxides on membrane substrates has proved to be an effective way to fabricate commercially available UF or NF membranes to get tight UF/NF ceramic membranes. The main advantage of this technique is controlled deposition of a monolayer of metal oxides.

This project was done to study the effect of ALD on 0.5 m long tubular membranes. TiO_2 was deposited on the membranes by means of atmospheric pressure atomic layer deposition (APALD). This is different from most of the reported studies that use vacuum-based ALD. $TiCl_4$ and H_2O were used as the main precursors for depositing TiO_2 through 2, 3 or 4 cycles of APALD. The growth rate of the deposited layer per cycle under different experimental conditions was measured indirectly using silicon wafers through ellipsometry. The effect of ALD was determined by measuring the membrane permeability and molecular weight cut-off (MWCO) values of the membranes before and after coating.

The results obtained showed a variation in growth rate per cycle (GPC) of the deposited layers for different experimental conditions. APALD was performed on 6 membranes and the GPC rate was acceptable for only 2 membranes (0.14 nm/cycle and 0.03 nm/cycle), whereas the GPC for the other membranes was very high (more than 1 nm/cycle). After deposition, the 2 membranes with acceptable GPC rate showed a decrease in MWCO value by 627 Da and 405 Da respectively. These results demonstrated that APALD could be used to fabricate ceramic membranes, but only at proper experimental conditions for TiO_2 deposition. An improved Carman-Kozeny model was also developed based on the MWCO value and on the GPC value, in order to predict the porosity and the permeability of the membranes. The results of the model and the measured permeability were compared; for some membranes, the model predicted correctly the permeability after coating.

Table of Contents

1. Introduction

The surface of the earth is mostly covered with water (around 71%) and most of the water is stored in oceans in the form of saline water (96.5%). The remaining amount of water (3.5%) is stored in freshwater lakes, glaciers, and polar ice caps in the form of ice (Williams, 2014). So, though being the most abundant resource on earth only a small percentage can be used by human beings to survive, and many areas in the world suffer from zero access drinking water that is clean and safe (Lee, Wu & Li, 2015). Rapid increase in population, increased industrialization and agricultural needs have resulted in continuous growth of the global water consumption rate (Lee, Wu & Li, 2015). This increase in freshwater demand and depletion of usable freshwater resources has made water scarcity a global issue (Song et al., 2016). The increase in water scarcity will cause rise in water price and that will affect the operating costs of many industries where water is used in a large amount (Lee, Wu & Li, 2015). Therefore, it is of high importance to develop water treatment technologies that are energy-efficient can purify water from various sources. In the past decades membrane technology has shown to be highly efficient and low cost water purification technique having application in various fields such as purification and separation of any substance, storage and conversion of energy, etc (Li et al., 2011).

In filtration processes membrane technology is used for ultrafiltration (UF), microfiltration (MF), reverse osmosis (RO) and nanofiltration (NF). Filtration of water by membrane is based on size-sieving mechanism, where the membranes reject substances having size bigger than the pores of the membrane whereas the rest pass. Use of membrane to perform microfiltration, ultrafiltration, nanofiltration and reverse osmosis are pressure driven (Reader: Micro- and ultrafiltration, Drinking Water Treatment, TU Delft). Polymeric/organic membranes are commonly used in many fields, but in the recent years ceramic/inorganic membranes has gained popularity due to its advantages over polymeric ones (Shang et al., 2017). The membrane materials used in the industries are porous, and their separation performance, such as rejection of a particular compound and permeability, are dependent on the size of the pores, pore size distribution and surface chemistry of the pores (Wang et al., 2013, Li et al., 2011). By changing the operational conditions and parameters involved in the

manufacturing processes, the membrane pore size can be controlled. However, the range of such operational changes is very limited and cannot be used to produce commercial membrane products in large quantity (Li et al., 2011). Therefore, a post-modification technique can be used to change the surface properties and the pore size of the membrane substrate. Post modification techniques are more flexible and convenient to manufacture membranes required for specific purposes and having diverse applications (Ulbricht, 2006).

A lot of techniques available for the fabrication of both polymeric and ceramic membranes are based on the reactivation of the surface-active groups present on the pore walls through chemical reactions. One of such technique is grafting, where the polymeric membrane substrate is first activated by chemical treatments or high energy irradiations based on the chemical nature of the membrane materials. Grafting can also be used for fabrication of inorganic membranes by linking molecules onto the hydroxyl groups present on the membrane surface through surface initiated polymerization or coupling reactions (Popat et al., 2004, Li et al., 2011). However, the chemical grafting technique is not a universal method, because it is specific to the chemical nature of the substrate membranes, and can work on some important membrane materials (Xi et al., 2009, Li et al., 2011). Also, this technique is tedious, time-consuming, cost-inefficient and uses a lot or organic solvents. Since this surface grafting reaction takes place in solutions, there is risk of not proper pores penetration or pore blocking during the drying step (Alf et al., 2010). So, in order to overcome the problems associated with chemical graft, other pore modification techniques were developed that are not dependent on the chemical reactivity of membrane materials. These techniques include sol-gel deposition, electroless deposition, atomic layer deposition (ALD) and chemical or physical vapor deposition (CVD or PVD) (Li et al., 2011). In these techniques a solid inorganic or polymeric layer is deposited in the pores of the membranes, and the deposited layer thickness can be changed to a lager range compared to chemical grafting layer. These deposited layers reduce the pore size of the membranes and also creates a new membrane surface (Li et al., 2011).

Between the above mentioned deposition techniques, ALD proved to be quite unique and distinctive owing to high conformality and uniformity of the deposited layers and precision in thickness control up to sub-angstrom level (George, 2009;

Grigoras, Airaksinen & Franssila, 2009). In ALD, thin layers of metallic oxides are deposited on substrate membranes through self-limiting gas-solid surface reactions (Li et al., 2011). A detailed explanation of the ALD process and its advantages over the other deposition techniques are given in section 2.5.

ALD has been mainly used in porous materials fabrication, such as nanomaterials, catalysts, optoelectronic materials,(Losic et al., 2006; Alessandri et al., 2009; Narayan et al., 2010); however, in the recent reports have shown its application to modify or functionalize porous ceramic membranes (Shang et al., 2017; Li et al., 2012; Chen et al., 2018). These reports showed that ALD is an effective method to reduce the pore size of the ceramic membranes, thereby developing tight nanofiltartion/ultrafiltration ceramic membranes with high level of permeability and better rejection capacity.

2. Literature Review

2.1 Development of Ceramic Membranes

A membrane can be defined as a semi-permeable barrier (active or passive), which under some driving forces removes one or more compounds present in a liquid mixture while the remaining is allowed to pass (Lee, Wu & Li, 2015; Wenten, 2002). The various driving forces include- pressure difference (used in ultrafiltration, microfiltration, etc.), difference in concentration (used in pervaporation, gas separation, etc.), electric (used in electrodialysis) and thermal (used in thermo osmosis, membrane distillation, etc.). A membrane can be solid or liquid physically (Wenten, 2002). The concept of synthetic membrane was first demonstrated by French Abble Nollet in 1748 where he showed that in animal bladder, wine was less semi-permeable than water. The first industrial scaled membrane was manufactured by Sartorius Werke GmbH, Germany in 1950 where they developed microfiltration membranes. Before 1950, manufactured membranes for filtration purposes were available but it was small scale and had its application only in laboratories. The major development in the field of membrane technology came back in late 1950s when thin membranes were discovered by Loeb and Sourirajan for reverse osmosis (Wenten, 2002).

Generally, membranes used in the various fields are made up of polymeric or inorganic materials. Membranes used in water treatment are commonly polymeric and used for micro-filtration, ultrafiltration, nanofiltration and reverse osmosis (Gitis and Rothenberg, 2016). In order to extend the use of membranes in aggressive media, such as alkali solutions, in wastewater treatment and industrial water treatment, membranes with higher chemical, mechanical and thermal stability are required (Condom et al., 2004, Skluzacek et al., 2007). Therefore, ceramic membranes can be a good option in such situations, as reports have shown that ceramic membranes have high thermal and chemical resistance and high mechanical strength, as raw ceramic material. Ceramic membranes can with stand temperatures like 500^0C and extreme pH-values (pH 1-14) (Benfer et al., 2001; Laitinen, 2001; Liu, 1996 and Shang et al., 2017).

In the past, the application of ceramic membranes were less numerous compared to polymeric membranes, as the fabrication cost was high and the packing density was lower (Gitis and Rothenberg, 2016; Laitinen, 2001 and Yacou et al., 2013). However, due to development by the industrial R&D, the fabrication costs decreased (Gitis and Rothenberg, 2016). Also, good packing density were obtained with some modules: multi-channel monoliths and hollow fiber configurations. Reports have shown packing density of round 1000 m^2/m^3 for hollow fiber membranes and 782 m^2/m^3 for multi-channel tubes configuration (Bhave, 2012; Lee, Wu & Li, 2015).

2.2 Structure and Characteristics of Ceramic Membranes

The structure of a ceramic membrane typically consists of 3 main layers - a porous support layer, an intermediate layer and a top/separation layer, as shown in figure 2.1. The thickness of the support layer is around few millimeters and the pores have size between 0.5-10 µm. This support layer is responsible for providing mechanical strength to the membrane. After the support layer comes the intermediate layer, with a thickness in the range 10-100 µm, that behaves as a transition phase and prevents the top layer from penetrating into the support layer. The pores in the intermediate layer are smaller than that of support layer, with a range of 0.05-0.5 µm. Finally, the top or separation layers, which plays the major role in filtration. The thickness of the top layer is between 1-10 µm, and the smallest pore diameters, between 2-50 nm (Babaluo et al., 2004).

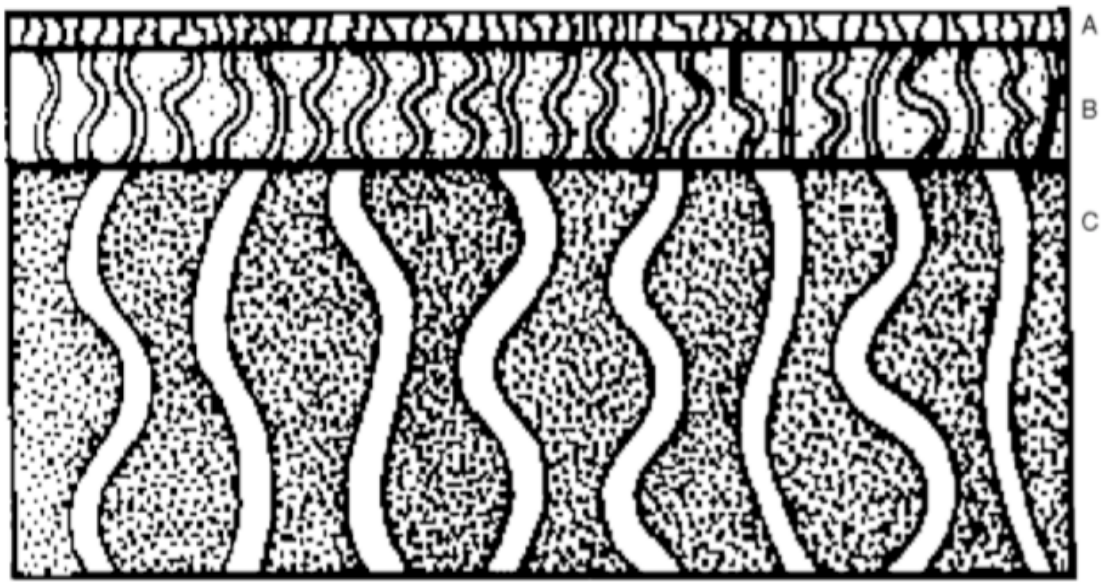

Figure 2.1: Schematic representation of the three layers of a ceramic membrane: (A) top/separation layer, (B) intermediate layer, and (C) support layer (Babaluo et al., 2004)

Based on the structure and morphology, ceramic membranes can be classified as porous and non-porous (dense) membranes, as shown in Figure 2.2. Porous membranes are made up of a ceramic support layer, mainly consisting of alumina, onto which additional porous layers are deposited. These layers at the top of support layer have different morphology and structure (Figure 2.2(b)). The top layers are mainly made up by deposition of silica, alumina or zirconia, with decreasing pore size from the support layer until the desired separation pore size (Bhave 2012; Kayvani Fard et al., 2018). Depending on the pore size, porous membranes can be classified into 3 groups, shown in Table 2.1.

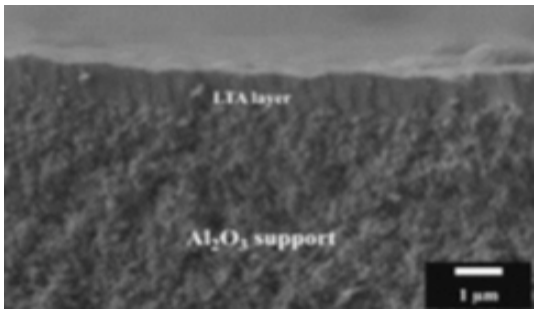

(a)

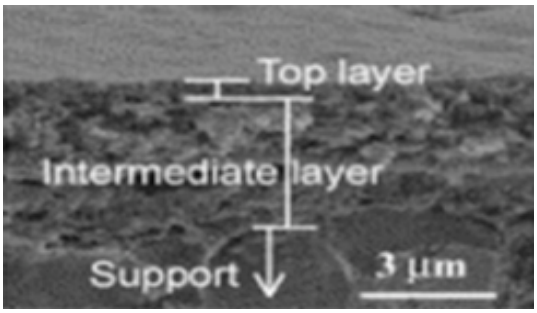

(b)

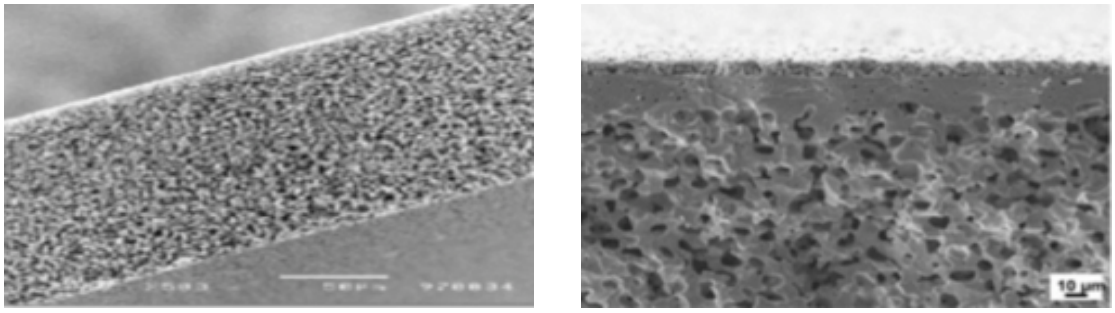

(c) (d)

Figure 2.2: Scanning electron microscope image of (a) dense, (b) porous, (c) symmetric and (d) asymmetric ceramic membrane (Kayvani Fard et al., 2018)

Table 2.1: Ceramic membrane types as per size of pores and permeation mechanism (Kayvani Fard et al., 2018)

Porous Membrane	**Pore size Diameter (nm)**	**Applications**	**Permeation Mechanism**
Microporous	<2	Gas separation + NF	Molecular sieving
Mesoporous	2-50	NF + UF and gas separation	Knudsen diffusion
Macroporous	>50	UF/MF	Poisseuille flow

Dense or non-porous ceramic are made of solid layers of metals (Pd, Ag, alloys) or solid electrolytes. They may have a support layer consisting of immobilized liquid (ceramic supports) that fills the pores in the membrane and create a semipermeable layer (Figure 2.2 (b)) (Hsieh, 1996).

Porous and non-porous membranes are again classified into symmetrical or asymmetrical membranes (Figure 2.2 (c) and (d)). In a symmetric membrane, the separation layer is similar compared to the other layers, whereas in asymmetric membrane the separation layer and the supporting layer can be distinguished (Kayvani Fard et al., 2018).

Ceramic membranes are commonly made of alumina (Al_2O_3). Generally, these membranes are porous and asymmetric and have a support layer with thickness between 1-3 mm. Two common geometries of ceramic membranes are tubular and flat (Laitinen, 2001; Larbot, 1996; Bonekamp, 1996 and Guizard et al., 2001).

Ceramic membranes used for filtration processes mainly operate under cross-flow filtration mode in order to maintain high filtration rate (Sondhi et al., 2003).

2.3 Application of Ceramic Membranes

Ceramic membranes can be used in the field of biotechnology, pharmaceuticals, dairy, food and beverages, petrochemical, drinking water and wastewater treatment plants (Sondhi et al., 2003). Owing to their high chemical and thermal stability along with high mechanical strength, ceramic membranes are widely used in chemical, food and textile industry (Combe et al., 1997). This report will focus on liquid separation by ceramic membranes. For liquid separation ceramic membranes are mainly used for microfiltration (MF) (50 nm – 1 um), ultrafiltration (UF) (2 – 50 nm) and nanofiltration (NF) (< 2nm). Figure 2.3 shows the application of ceramic membranes in various filtration processes according to their pore size, molecular weight and the corresponding applications with regard to the target compounds to be removed.

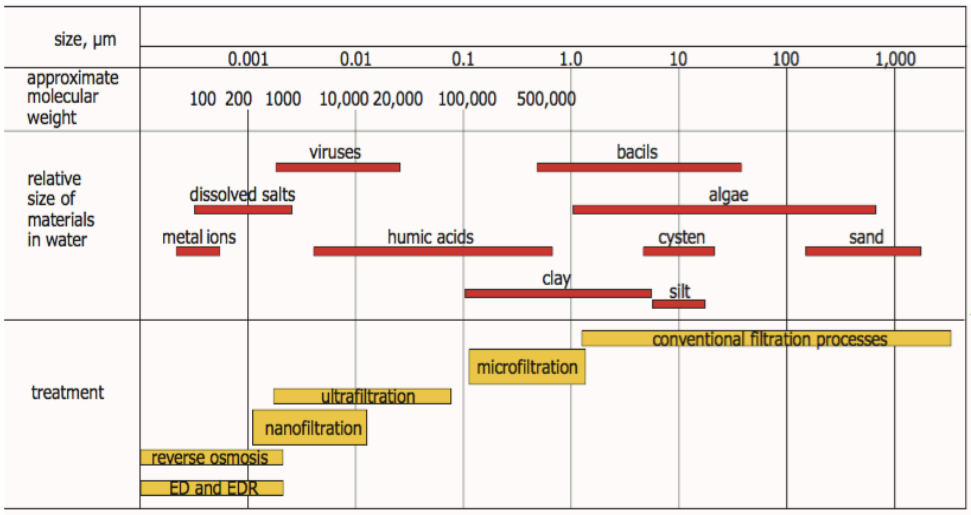

Figure 2.3: Type of ceramic membrane and application
(Source: Micro- and ultrafiltration, Drinking Water Treatment, TU Delft)

Application of MF ceramic membranes has been shown in juice and sugar production, treatment of oily wastewater and sterilization of pharmaceuticals (Sondhi et al., 2003; Chang et al., 2014; Luque et al., 2008). Based on their pore size ceramic MF membranes can be used to remove particles such as sand, clay, giardia, cryptosporidium, algae, and some bacteria, but not viruses from a liquid medium. Ceramic UF membranes having pore sizes between 2-50 nm can be used to remove

much smaller materials compared to MF membranes. They can be used to remove bacteria, most viruses and proteins based on sieving mechanism as well as electrostatic repulsion.

Ceramic membranes can also be used for NF and RO processes. Ceramic NF membranes can be used to remove any type of bacteria or viruses. They can also remove carbonates, bicarbonates, multivalent ions, and compounds responsible for the toxicity of water (Dasgupta et al., 2015 and Chon and Cho, 2016), but they do not reject monovalent ions. In RO membranes all compounds present in the water are being rejected, including monovalent ions, but in RO membranes the raw water requires pre-treatment by MF/UF membranes. This pre-treatment is required as RO membranes are very sensitive so they can get easily degraded without it (Biron et al., 2018 and Gu et al., 2016). The main objective of RO membranes is desalination of seawater (Biron et al., 2018).

2.4 Fabrication of Ceramic Membranes

The fabrication steps of ceramic membranes are (a) ceramic powder paste (suspension) preparation, (b) shaping of ceramic powder into required geometry, (c) heat treatment consisting of calcination and sintering (Li, 2007). In addition to the above steps, additional layer deposition such as dip-coating, CVD, sol-gel and ALD can also improve membrane selectivity and properties. The methods or processes used for different fabrication steps depend on various factors, such as membrane configuration, final chemical and mechanical strength, selectivity of the fabricated membrane, morphology and quality of the membranes (Lee, Wu & Li, 2015; Li, 2007).

2.4.1 Preparation of the Ceramic Powder Paste or Suspension

In this stage the raw inorganic material are processed to desired shape and size. Normally, the raw ceramic powder is transformed into a paste or suspension in order to get the required shape with ease. Some additives are also added in this step to influence the membrane's microstructure and quality. Additives such as fatty acids and esters helps in stabilizing the ceramic particles in suspension which in turn gives high particle loadings and high quality ceramic membranes (Lee Wu & Li, 2015, Li

2007, Calvert et al., 1986).

2.4.2 Shaping of Ceramic Paste

After the paste or suspension formation stage comes the shaping stage, where the ceramic paste is transformed into the required shape by means of various processes. The processes involved in shaping are: tape casting, pressing, extrusion, slip casting, foam and leaching techniques, phase inversion (Lee Wu & Li, 2015).

Pressing is the most common way to make flat ceramic membranes. A force ranging from 10-100 MPa is applied over an area until the ceramic particles are consolidated (Silva et al, 2012; Xin et al., 2007; Drioli & Giorno, 2010). Membranes produced by this method have symmetric structure as the force is applied uniformly over the area of ceramic material (Lee Wu & Li, 2015). Disc membranes are commonly formed by this method (Lee Wu & Li, 2015).

Tape casting is used to prepare flat ceramic membranes. In this method, the ceramic paste or suspension is taken into a reservoir, which is controlled by a blade that can be height adjusted over a carrier film. The gap between the blade and carrier determines the thickness of the membrane. After that the suspension is dried in a controlled environment (Lee Wu & Li, 2015).

Slip casting is used to prepare tubular ceramic membranes. In this method a porous mould is used to get the required shape. The ceramic paste is poured into the mould and under capillary force the solvent present in the paste goes out through the pores in the mould. The ceramic particles left on the surface of the mould gets consolidated to form a layer of particles or a layer of gel (Lee Wu & Li, 2015).

Extrusion is used to produce hollow-fibre/capillary, monolith and tubular membranes. This process consists of an orifice of desired shape through which the suspension paste is forced and consolidated under high pressure. To get hollow tubes the paste is forced through a die under pressure around 20MPa (Lee Wu & Li, 2015).

2.4.3 Heat Treatment after Shaping

After giving shape to the ceramic paste or suspension, the ceramic membrane

precursors are formed, which are then dried by application of heat to get the final product. The main processes involved in the heat treatment step are: pre-sintering, thermolysis and final sintering. The main objectives of this heating step are to remove any materials present in the paste other than ceramic material, to give the membrane the required strength and to define the final dimension and microstructure of the membrane.

Pre-sintering takes place at temperature around 200^0C and is used to remove any form of water present in the ceramic precursors. After pre-sintering, thermolysis is done to remove any organic matter in the precursor and after that final sintering is performed. Final sintering is the most important stage in the heat treatment processes, as in this stage the shape characteristics of the membrane (i.e.: size of the pores and porosity) are defined, and the final shape and mechanical strength is obtained. Higher the sintering temperature higher will be the mechanical strength and lower will be the porosity of the membrane (Lee, Wu and Li 2015, Li 2007).

2.4.4 Additional Layer Deposition

The fabrication methods discussed above produce ceramic membranes having pore size greater than 1μm. But if we need membranes of pore size less than 1μm, deposition of addition layers of ceramic particles, intermediate layers and a top membrane layer, having different sizes are necessary (Gitis and Rothenberg, 2016). These depositions help in obtaining gradient pore structure across the membrane cross-section and can be done by one of the methods: dip coating, sol-gel method, CVD or ALD. This additional layer deposition helps in improving membrane properties such as selectivity, porosity, hydrophilicity, conductivity, permeability (Lee, Wu and Li 2015).

Dip Coating

Dip coating is commonly used to deposit top and intermediate layers on the support layer. In this method the support layer, which is dry and porous, is dipped into a suspension consisting of ceramic powder and then taken out from the suspension. The change in pore size of the final membrane can takes place in two ways. First, the suspension is deposited on the substrate surface by rotating the substrate, thereby

forming a layer of well-defined thickness. Second, after taking out from the suspension, the liquid can be sucked into the pores of the support under capillary forces (Babaluo et al., 2004; Lee, Wu and Li 2015).

Sol-Gel method

Sol-get method is used to fabricate UF and NF ceramic membranes having pore size in between 1-100 nm (Das and Maiti, 2009). A sol generally consists of a polymeric solution or a colloidal solution of alkoxide, which is deposited on the membrane substrate through dip coating. This colloidal solution is then converted into a gel form by hydrolysis and condensation or polymerization. At the end heat treatment is given to form a thin and uniform layer over the membrane (Lee, Wu and Li 2015).

Chemical Vapor Deposition (CVD)

CVD method is used to fabricate ceramic membranes having pore size less than 1 nm (Labropoulos et al., 2014). It is an efficient way to decrease the pore size of ceramic membranes to get tight UF and NF properties. In this method, one or more volatile precursors such as silicon dioxide or metal dioxide in gaseous phase are exposed together on porous substrate at high temperature and in vacuum environment (Drioli et al., 2017). The solid materials are converted to gaseous phase due to chemical reaction between volatile precursors and the surface to be coated. This resulting chemical reaction forms a solid phase and gets deposited on the substrate (Makhlouf, 2011).

Atomic Layer Deposition (ALD)

Atomic layer deposition is a self-limiting gas-phase deposition process where films of oxides, polymers, metals, etc., having thickness in the atomic scale level, are deposited on support substrate (Shang et al., 2017; Li et al., 2012). In this method two precursors are pulsed one after another separately in the gas phase. A purge step is provided with inert gas in between the applications of two precursors so as to remove any unreacted precursors or by-products (Li et al., 2012; Marichy et al., 2012). A detailed explanation of ALD is given in section 2.5.

2.5 Application of ALD on Ceramic Membranes

The ALD process was first introduced in 1970s; back then it was known as "atomic layer epitaxy (ALE)", and was used to deposit ZnS for electroluminescent displays. In 2000s the semiconductor industry started using the same technique to develop polycrystalline or amorphous materials, and the name changed from "epitaxy' to "deposition" (Koutsonikolas et al., 2017). ALD is commonly used to fabricate various porous materials such as nanomaterials, catalysts, optoelectronic materials, etc (Li et al., 2012). However, in recent years, reports have shown its application in fabrication of ceramic membranes (Shang et al., 2017; Chen et al., 2018; Li et al., 2012).

ALD is a layer deposition technique where chemical precursors are exposed alternatively on a proper substrate. For ceramic membranes, ALD can be used to deposit porous materials like TiO_2, SiO_2 or Al_2O_3 in a layer-by layer way. The ALD process consists of consecutive use of self-terminating gas-solid reactions known as half-reaction. At the first half-reaction, the first precursor is pulsed into the ALD chamber, that contains the selected membrane substrate, for a particular amount of time; during this time the precursor can react completely with the substrate surface. This results in the formation of a monolayer on the surface. Then, gases like N_2 or Ar are used to purge the reaction chamber. Purging is done to remove any unreacted precursor or reaction by-products. After the purging step, the second precursor is pulsed followed by purging again completing one cycle. After one cycle, one layer of the desired material is formed. This deposition process is then repeated for a number of cycles depending on the growth rate per cycle (GPC) of the deposited material in order to get the required thickness of the deposited material (Koutsonikolas et al., 2017; Kemell et al., 2008). A schematic representation of the various steps involved in getting one cycle of ALD is shown in figure 2.4.

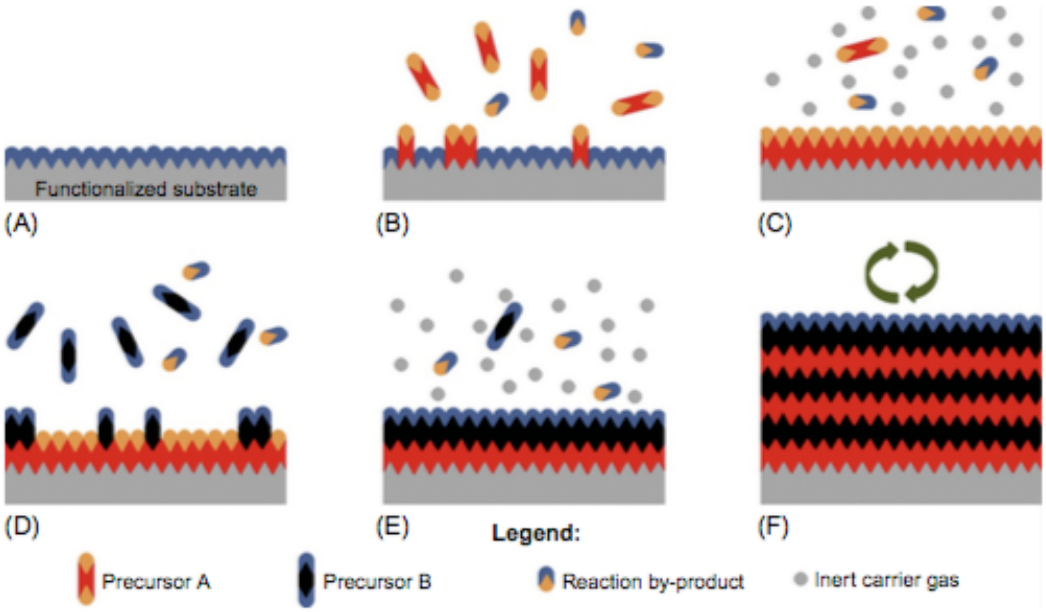

Figure 2.4: Schematic representation of deposition of film during ALD process. The scheme shows (A) substrate with reactive sites, (B) first precursor is pulsed, (C) purging of by-products and unreacted precursor, (D) second precursor is pulsed, (E) purging of by-products and unreacted second precursor, and (F) film resulting from several ALD cycles (Koutsonikolas et al., 2017)

Compared with CVD and other post-fabrication techniques, where the precursors are introduced together simultaneously into the reaction chamber that contains the substrate to be fabricated, , ALD has the following advantages to fabricate porous materials (Malm et al., 2011). Firstly, as both the precursors that are used in ALD are in gaseous state, they can easily enter into the small pores, and get adsorbed on the pore wall or react with the precursor adsorbed before. Secondly, the surface reactions in ALD are alternating and self-limiting, so coatings are highly uniform and conforming. Thirdly, ALD provides better control of the deposited layer thickness by adjusting the number of deposition cycles. Finally,a large number of compounds (such as sulfides, oxides, metals and polymers) can be deposited on membrane substrates made of polymers, ceramics or biomolecules (Li et al., 2011; Shang et al., 2017).

Three factors that can affect the deposition of atomic layer by ALD: purge time, deposition temperature, and number of cycles.

The purge time should be long enough to guarantee that there is no previous precursor or any by-products left. Without a proper purge time CVD may happen in the free spaces present in the reaction chamber, which will result in formation of densely packed particles instead of conformal and uniform thin films on the membrane substrates (Kemell et al., 2008).

The deposition temperature controls the growth rate of deposited thin film on the substrate. For a self-limiting film growth, the temperature should be in the range of "growth window". If the working temperature is too low, there may be decrease in the growth rate due to low precursors reactivity or increase in the growth rate owing to condensation of excessive precursors on the substrate surface. If the temperature is too high, it may cause decomposition of the deposited film due to side reactions of the by-products, precursor particles or layer etching effect, called desorption (Boryło et al., 2018).

The number of cycles influences the thickness of the deposited layer. Although the thickness of the thin deposited layer should increase with increase in the number of ALD cycles. But in practice, the geometry of the substrate surface affects the thickness as well. For ALD on porous materials, the precursors cannot diffuse into pores after a certain number of cycles due to development of cover film on the top (Li et al., 2012).

3. Thesis Research Framework

3.1 Problem Statement

As ceramic membranes have high mechanical strength and high thermal and chemical stability over polymeric ones, the use of tight ceramic UF/NF membranes are gaining importance (Mori et al., 1998; Shang et al., 2017). These tight membranes have greater selectivity owing to their small pore size, but there are some problems associated with it. First, as the selectivity gets high, the permeability gets low. This decrease in flux can be rectified by decreasing the membrane thickness but the risk of forming defects increases, which in turn affects the selectivity (Spillman, 1995; Sengupta & Sirkar 1995). Second, the fabrication of these membranes requires higher control over the structure and thickness of the membranes, because with decrease in pore size the membranes are more prone to micro cracks. These micro cracks can badly affect the filtration efficiency of the membranes (Burggraaf & Cot, 2009).

3.2 Objective of the Research

Based on the problems defined above, it is required to use a fabrication technology that deposits a thin-film layer of metal oxides on the top layer of the membranes and reduce the pore size in a more controllable and standardized way, without causing defects and severe permeation loss. ALD has been shown as a promising modification technology to produce better separation layer for ceramic membranes. Study by Li et al., 2012 has shown that ALD is an effective tool to precisely tune the pore size of the ceramic membranes and to control deposition of the metal oxide layer. ALD has also proved to fabricate tight NF ceramic membranes, which showed better rejection with limited loss in permeability (Shang et al., 2017; Chen et al., 2018). The objective of this research is to check the implication of this technique on the characteristics of 0.5 m long tubular ceramic membranes.

3.3 Research Question

For achieving the objective of this research, the following research questions were formulated:

1. What is the growth rate per cycle (GPC) of the ALD based on the experimental conditions? GPC is the thickness of the atomic layer deposited after one cycle of ALD.

2. What is the change in permeability and molecular weight cut-off (MWCO) of the coated membranes when APALD is applied? MWCO is a measurement of the selectivity of a porous membrane and is defined as the molecular weight of the spherical molecules that are 90% rejected by the membrane pores (Reader: Micro- and ultrafiltration, Drinking Water Treatment, TU Delft).

4. Materials and Methods

4.1 Substrate Membranes

For this research, 12 tubular membranes (M1, M2…M8, M10...M13) having length of 50 cm, inner diameter 8 mm and outer diameter 10 mm are used (figure 4.1). The membranes were purchased from the company Hongyi Ceramic Membranes located in Nanjing, China. All the membranes are coated with epoxy glue on both the ends to prevent the filtration at the ends. As per the company, the supporting layer is made up of alumina (Al_2O_3) while the separation layer is made up of titanium dioxide (TiO_2). The effective filtration area of the membranes was calculated by taking filtration length of 42.5 cm and it was found to be 0.010676 m^2.

4.2 Epoxy Glue

The epoxy glue is put on the two ends of the tubular membranes in order to seal the edges of the membranes up to a length of 1-2 cm as shown in figure 4.1. The glue is prepared by mixing Araldite® AW 4804 and Hardener HW 4804 in the ratio 100:15 by weight. The key properties of the glue are it has excellent heat resistance up to 210^0C after post-cure, its self-leveling, it has good environmental resistance and long pot life. Before application of the glue, the membrane edges were cleaned with acetone for removing any traces of oil, grease and dirt. After application of glue on the edges, it was allowed to harden in atmosphere for 3 hours first then it was put in an oven for 2 hours at 120^0C. The membranes were not put directly into the oven at 120^0C, they were put when the oven temperature was around 30-40^0C and the temperature rose with time. The 2 hours in the oven was counted from the moment when the temperature reached 120^0C.

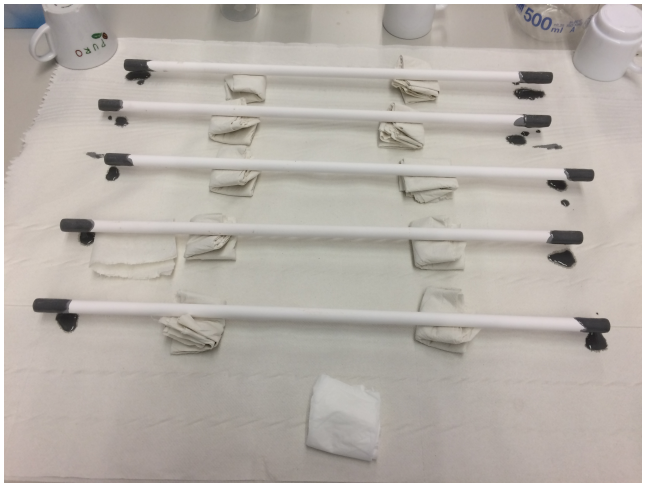

Figure 4.1: Application of Epoxy glue on the edges of the tubular membranes

4.3 Membrane Characteristics and Performance

In order to determine membrane characteristics and performance, permeability and molecular weight cut-off (MWCO) of the membranes based on PEG rejection are measured before and after ALD. The membranes obtained from the company are dry and wrapped, so cleaning was not done. Before performing the tests the membranes were soaked in ultrapure water for a period of 24 hours. After performing the permeability and MWCO tests, the membranes are cleaned with 0.2 % (by weight) of NaOCl (Boom Laboratoriumleverancier). The permeability values, before and after chemical cleaning are compared. Chemical cleaning was repeated until the permeability values before and after cleaning were almost similar. After chemical cleaning, the membranes were kept in ultrapure water.. Before sending the membranes for ALD, the membranes were completely dried by keeping them in the oven at 120^0C for 12 hours. After ALD coating, the permeability and MWCO test were repeated and the results before and after ALD were compared.

4.3.1 Experimental Setup

The image and schematic view of the experimental setup are shown in figure 4.2 and 4.3 respectively. The setup is a cross-flow filtration system with a circular loop, where the concentrate is fed back into the feed tank. The setup has of two feed tanks of 50 L; one contains demi-water and the other contains a Polyethylene Glycols (PEGs) solution. Further, the setup consists of a pump, membrane casing, valves, two pressure meters, flow meter, and temperature meter. The ultrapure water used for the

permeability test was taken in a separate jerrycan and feed into the setup. The demi water tank and the PEG solution tank were used for the MWCO test. When one tank is used for the feed water, the other tank is kept closed using valves. The pump was used to allow the flow the water from the tanks/jerrycan to the entire system and to get the required trans-membrane pressure (TMP), together with a pressure valve. The cross-flow velocity, feed flow pressure and concentrated flow pressure were measured with sensors. The temperature of water in PEG tank/jerrycan was also measured..

The system was linked to Labview software, which controlled the speed of the pump, the opening of valves, and showed the flow and pressure measured by sensors.

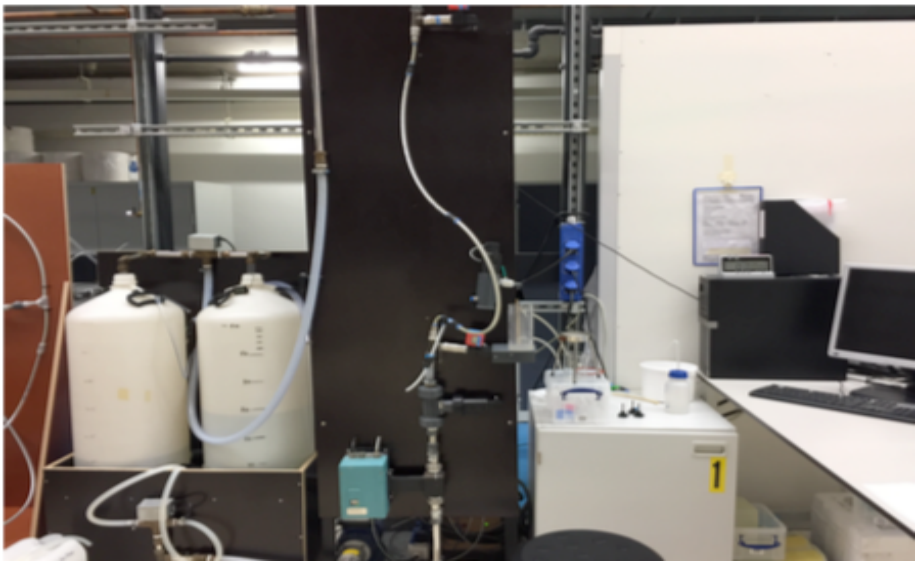

Figure 4.2: Picture of the filtration setup in the lab

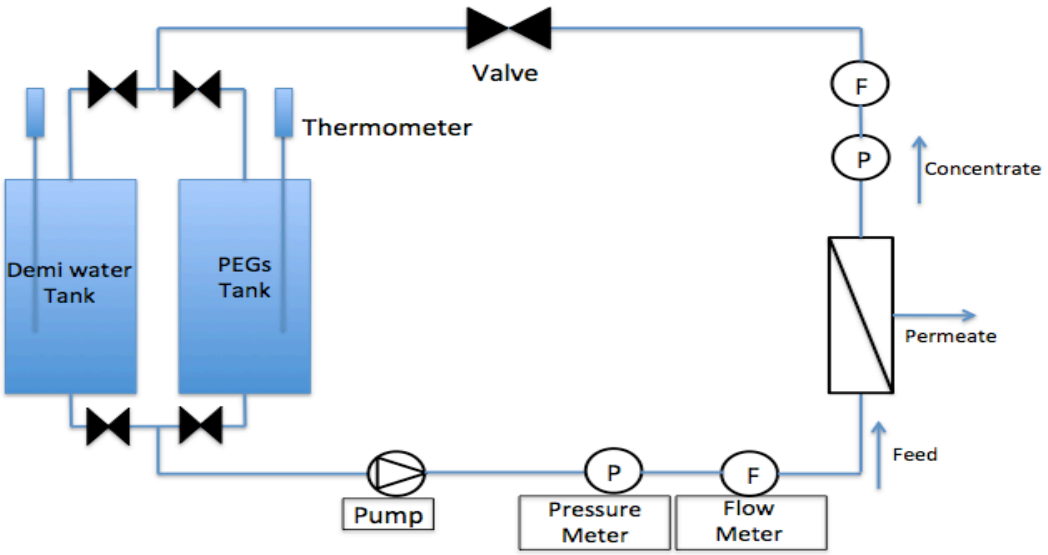

Figure 4.3: Schematic view of the filtration setup

4.3.2 Water Permeability

Permeability of a substance can be defined as its ability to transmit any liquid. For ceramic membranes it is the capacity of the membrane to allow the liquid to pass through its pores under a constant pressure and temperature. In this research, the permeability of the membranes has been measured using, ultrapure water under a constant trans-membrane pressure (TMP) of 3 bar and room temperature. The pump cross flow was maintained around 175 L/hr. The entire experiment was run for 20 minutes and 3 samples were collected during this duration. The first sample was collected after 5 minutes from the starting time and the next two were collected at an interval of 5 minutes. The temperature of the feed water was monitored throughout the experiment and it was observed that with experiment running time the feed water temperature was rising. This rise in temperature was due to heat transfer from the cross flow pump and so the permeability was corrected for temperature and the corrected permeability at 20^0C was measured using Eq. 4.1 (Shang et al., 2017).

$$L_{p,20^0C} = \frac{J.e^{-0.0239\,(T-20)}}{\Delta P} \qquad \text{Eq. 4.1}$$

$$J = \frac{Q}{A}$$

where,
$Lp_{20°C}$ - Permeability at 20°C (L.m^{-2}.hr^{-1}bar^{-1});
J - Membrane Flux (L.m^{-2}.hr^{-1});
T - Temperature of the feed solution (°C);
ΔP - Measured TMP (bar).
Q - Flow rate (L/hr)
A - Effective filtration area (m^2)

The flow rate was determined using the following equation.

$$Q = \frac{W_2 - W_1}{t} \quad \text{Eq. 4.2}$$

W_2 - Weight of permeate liquid and beaker (g)
W_1 - Weight of empty beaker (g)
t - Time (hr)

The average value of the permeability of the 3 samples is taken as the permeability of the tested membrane.

4.3.3 Molecular Weight Cut-off (MWCO)

For a ceramic membrane, the MWCO is the molecular weight (MW) of a tracer molecule in dalton (Da), which is rejected by the membrane by 90%. A mixture of polyethylene glycol (PEG) (SIGMA-ALDRICH, Germany) of different sizes was used as a feed solution for filtration experiments. The PEG sizes were 1000 Da, 1500 Da, 2000 Da, 3000 Da, 4000 Da and 6000 Da; for each size, the PEG concentration was 0.6 g/L. Since the PEGs are non-charged, the rejection mechanism by the membranes is steric hindrance. This means if the size of the PEG is bigger than the pores of the membrane, then they will be rejected otherwise they will pass through the membrane pores. The feed solution was fed into the membrane at a constant TMP of 3 bar under room temperature and at cross-flow velocity of 175 L/hr.

The setup was run for 50 minutes first and then 3 permeate samples were taken at an interval of 10 minutes. Other 2 feed samples were taken when first and last permeate samples were collected. The temperature was also monitored during the experiment. To determine the MWCO of the membrane, the feed and permeate samples of the membrane were filtered by a 0.45 μm filter (Macherey-Nagel GmbH & Co. KG) and then analyzed by a high performance liquid chromatography system

(HPLC, Shimadzu, Japan) containing size exclusion chromatography (SEC, 5μm 30 Å PSS Polymer Standards Service GmbH, Germany) columns.

In order to determine the MWCO of the membranes, a calibration graph was made for the various standard PEG solutions. 6 PEGs (1000-6000) solutions having concentration of 0.6 g/L each were prepared separately and analyzed by HPLC. The elution time of the various PEGs were determined from the HPLC results and a graph was plotted using a polynomial model showing the relationship between the elution time and molecular weight of the PEGs as shown in figure 4.4. From this calibration curve the retention curve of a PEG having a particular molecular weight can be plotted using Eq. 4.3 (Shang et al., 2017).

$$R_i(\%) = \frac{C_{i,feed} - C_{i,permeate}}{C_{i,feed}} \qquad \text{Eq. 4.3}$$

where

R_i (%) = Retention of PEG molecule i (in perentage)
$C_{i,\ feed}$ = concentration of PEG in feed solution (g/L)
$C_{i,\ permeate}$ = concentration of PEG in permeate solution (g/L)

Then a log-normal model was used to develop the experimental rejection curves, which is a function of MW and MWCO as shown in Eq. 4.4. (Shang et al., 2017)

$$\sigma\,(MW_s) = \int_0^{MW_s} \frac{1}{S_{MW}\sqrt{2\pi}} \frac{1}{MW} \exp\left[-\frac{(\ln(MW) - \ln(MWCO) + 0.56\,S_{MW})^2}{2\,S_{MW}^2}\right] dMW \qquad \text{Eq. 4.4}$$

where

$\sigma\,(MW_s)$ = Reflection coefficient (in %)
S_{MW} = Standard deviation of molecular weight retention (in Da)
MW = Molecular weight cut-off (in Da)

An example of modeling result for MWCO is shown in figure 4.5, where grey dotted line shows the data obtained from filtration test and the black line is the modeling result.

The average value of the MWCO of the 3 samples is taken as the MWCO of the membrane under consideration.

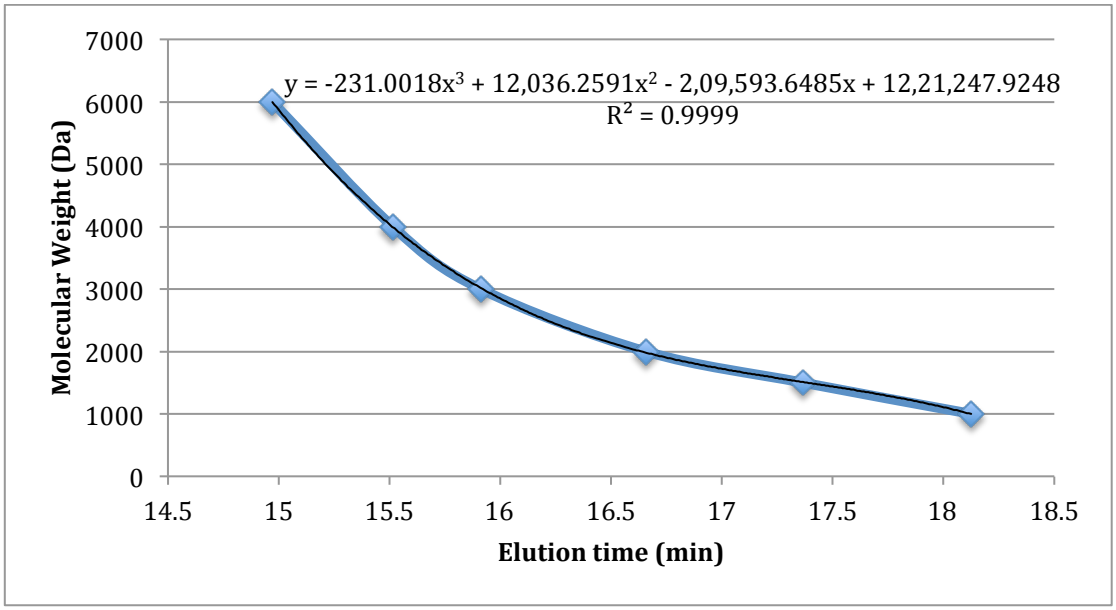

Figure 4.4: Calibration curve using PEGs with Molecular weight of 1000 Da, 1500 Da, 2000 Da, 3000 Da, 4000 Da and 6000 Da

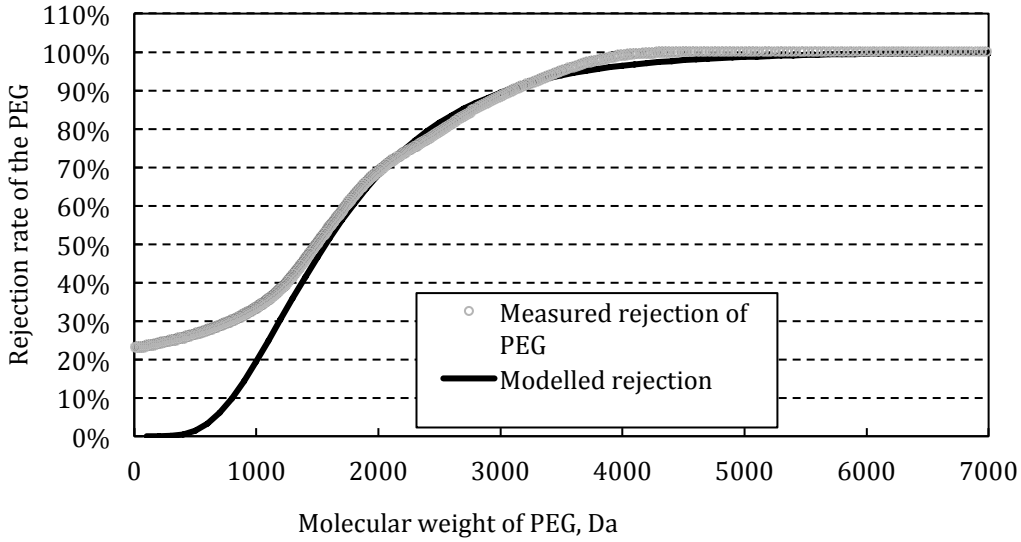

Figure 4.5: Graph for modelled and measured PEG rejection for a long tubular membrane

4.3.4 Application of ALD on the membranes

Out of the 12 membranes, 6 membranes (M1, M2, M4, M5, M11 and M12) were selected for application of ALD and the atomic layer deposited was TiO_2. The membranes were taken as a set of two: (M4, M2); (M1, M5); (M11, M12), and the experimental conditions were kept same for a chosen set except the ALD cycles. ALD

was performed on the membranes by a flow-type ALD reactor (Delft IMP B.V) at the company Delft IMP located in Delft and the type of ALD was atmospheric pressure atomic layer deposition (APALD). A schematic view of the reactor is shown in figure 4.6. Most of the studies where application of ALD on ceramic membranes was investigated used ALD under vacuum conditions (Li et al., 2012; Song et al., 2016). The main advantage of using APALD is that in this technique the use of expensive vacuum-compatible equipment is not required. As a result, this technique can be easily scaled for production in large volumes (Shang et al., 2017). For TiO_2 coating on the substrate membranes the membranes were fixed vertically in the ALD reactor. $TiCl_4$ and H_2O were used as precursors and N_2 as purge gas. The flow of precursors over the substrate was in a parallel direction to its surface. The surface reaction on the membrane substrate can be depicted in the following equations 2.5 and 2.6 (Shang et al., 2017).

$$n(\text{-OH})^* + TiCl_4\,(g) \rightarrow (\text{-O-})_n(TiCl)_{4-n}^* + nCH_4\,(g) \qquad \text{Eq. 4.5}$$

$$(\text{-O-})_n(TiCl)_{4-n}^* + H_2O\,(g) \rightarrow (\text{-O-})_nTi(OH)_{4-n}^* + (4 - n)HCl\,(g) \qquad \text{Eq. 4.6}$$

where * represent the surface species

$TiCl_4$ was the first precursor exposed to the membrane surface followed by purging with N_2 gas. As explained before, purging helped in removing the by-products formed and the residual $TiCl_4$. After purging, H_2O is introduced in order to have deposition of TiO_2. Purging with N_2 was again done after H_2O exposure thereby finishing 1 cycle. The entire ALD process was done automatically and the temperature of the reactor was maintained at 180^0C by using the infrared lamp as shown in figure 4.6. A probe connected to the lamp monitored the temperature. A heating pre-treatment of the substrates (both membranes and wafers) was included before the first coating cycle in order to ensure that any water molecules would be removed from the substrate. ALD was performed on a set of 2 membranes and the experimental conditions were kept same for the set. The various experimental conditions used for ALD on the 6 membranes are shown in Table 4.1.

Table 4.1: Experimental conditions of ALD on various membranes

	Temp. in Line A (^{0}C)	Temp. in Line B (^{0}C)	Time Preheat (min)	Time Prec A (sec)	Time purge A (sec)	Time Prec B (sec)	Time purge B (sec)
M4	100	100	20	10	1200	60	1200
M2	100	100	20	10	1200	60	1200
M1	180	180	45	7	1200	60	1200
M5	180	180	45	7	1200	60	1200
M11	180	180	60	7	1800	60	1800
M12	180	180	60	7	1800	60	1800

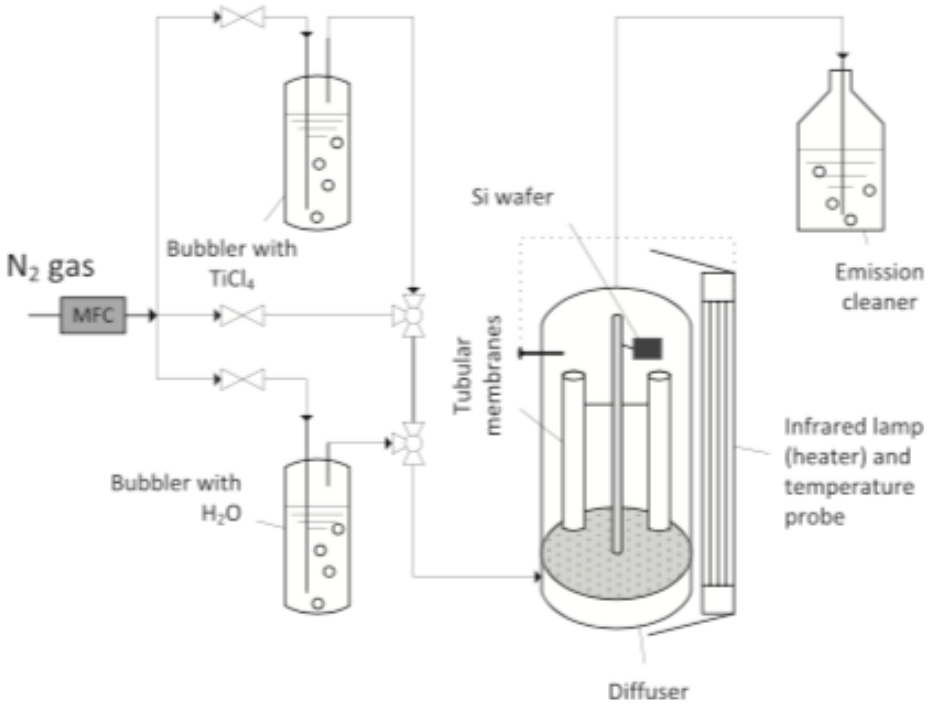

Figure 4.6: Schematic view of the ALD setup (Shang et al., 2017)

4.3.5 Growth rate of TiO_2

Ellipsometer (M-2000F, J.A. Woollam Co. Inc., USA) was used to measure the growth rate of ALD on the substrate membranes. Ellipsometry uses the principle of light polarization to measure the ALD thickness (Shang et al., 2017). However, as the membranes were tubular in shape, it is not feasible to directly measure the coating thickness on the curved surface of the separation layer (Shang et al., 2017). So silicon wafers of size 1.5 cm x 1.5 cm with flat surface were used to measure the growth rate

of ALD indirectly. During the application of ALD on the substrate membranes the wafers were put next to membranes at the top location in the reactor, so that the metal oxide also get deposited on the wafers. The wafer thickness was measured before and after coating by ellipsometry and then the growth per cycle (GPC) can be then calculated using Eq. 4.7. The thickness on the wafers was measured on 5 locations as shown in figure 4.7 and the average was taken to determine GPC.

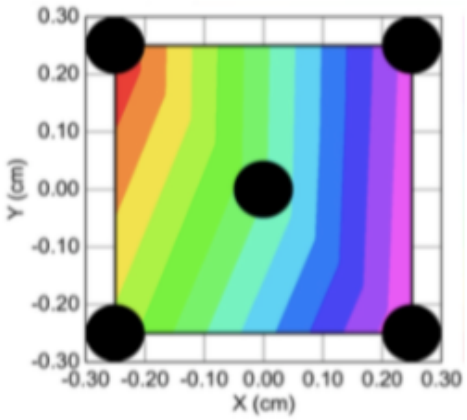

Figure 4.7: Measuring points on the wafers

$$\text{GPC} = \frac{d_2 - d_1}{A} \qquad \text{Eq. 4.7}$$

where,
d_1 = Thickness of layer before coating, nm
d_2 = Thickness of layer after coating, nm
A = Number of cycles

4.4 Development of Carman Kozeny Model

An improved Carman-Kozeny model was developed after the experimental studies to model the change in permeability values of the membranes after APALD. The permeability values were estimated by calculating the change in pore size of the membranes based on two methods: a) the MWCO value b) the GPC rate on wafers. As, the pore size of the membranes were not measured experimentally, so Eq. 4.8 was used to estimate the pore sizes based on the measured MWCO (Seader et al., 1998). A detailed explanation of the model is given in chapter 6.

$$D = 0.065\ (MWCO)^{0.438} \qquad \text{Eq. 4.8}$$

5. Results and Discussions

5.1 GPC of TiO_2 on silicon wafers

The GPC on the 6 membranes that were measured from the wafers kept alongside with the membranes during APALD are shown in table 5.1.

Table 5.1: Growth rate per cycle of the TiO_2 ALD on the membranes

Membrane Number	Number of Cycles	GPC (nm/cycle)
Membrane 2	3	12 ± 3.46
Membrane 4	2	4.7 ± 2.76
Membrane 1	2	0.92 ± 0.31
Membrane 5	3	1.32 ± 0.82
Membrane 11	3	0.141 ± 0.05
Membrane 12	4	0.030 ± 0.07

From Table 5.1 it can be seen that the GPC measured on the wafers for different membranes were quite different. These differences can be due to different precursors pulse time, purge time and number of cycles (Triani et al., 2006 and Puurunen 2005). Out of the 6 membranes, the GPC on set (M2, M4) showed the highest GPC rate compared to other membrane sets. This higher GPC rate could have resulted from higher pulse time of precursor $TiCl_4$ (10 sec) compared to the set of other membranes (7 sec). This longer pulse time could have resulted in adsorption of more precursors on the wafer surface and resulted in higher GPC (Chen et al., 2017). The experimental conditions for M2 and M4 were same; however, the GPC rate in them is quite different. This could have been due to difference in the number of ALD cycles. ALD changes the chemical composition of the substrate surface. In the first cycle, deposition occurs on the surface of the original substrate material, the following cycles usually on a surface with both the original substrate and the ALD-grown material exposed. When there is change in the chemical composition of the substrate surface, the GPC should be expected to vary with the number of cycles (Puurunen 2005). Another possibility can be that the ALD was not controlled properly, which resulted in deposition of monolayer of varied thickness at every cycle. As the thickness of the deposited layer was measured after a number of cycles, and not at each cycle, it is not possible to prove that the TiO_2 thickness deposited on

wafer at each cycle is constant. Also, the deposition of TiO_2 may not be uniform on the entire wafer surface; the GPC is based on the measurements of some points on the wafer, so there is possibility of some random errors while measuring the wafers before and after ALD through ellipsometry, which resulted in GPC variation.

For the other membrane sets (M1, M5) and (M11, M12), the GPC is low compared to (M2, M4). This could be due to lower precursor pulse time of 7 sec compared to 10 sec as mentioned before. However, for set (M1, M5) the GPC was quite high compared to the expected value and only the set (M11, M12) have shown acceptable GPC rate. The pore size of the membranes, calculated by equation 4.8, was around 2 nm. Therefore, a GPC rate of 1 nm/cycle is not acceptable because it may result in complete blockage of the pores with a few cycles. This high GPC rate of (M1, M5) could have resulted from lower purging time (1200 sec) compared to (M11, M12) (1800 sec). Due to lower purging time the unreacted precursors on the wafers for (M1, M5) might have not been removed properly from the wafers, resulting in a higher thickness of the deposited layer. Based on the GPC of the 3 membrane sets it can be said that the experimental conditions for the set (M11, M12) was the best in order to have proper tuning of the pore size through APALD.

Reports on ALD deposition of TiO_2 under vacuum conditions have shown GPC of 0.03-0.05 nm/cycle (Nevalainen et al 2012; Lei et al., 2013; Abdulagtov et al., 2012). In our study at atmospheric conditions, only M12 has shown a GPC in this range, while the GPC of all the other membranes is higher. In the literature, this has been explained as follows. First, vacuum conditions prevent the formation of precursor and co-reactant multilayers on the substrate surface, promoting lower GPC than in atmospheric conditions. Second, under atmospheric pressure, it is difficult to remove excess precursors and reaction by-products through purging (Shang et al., 2017). Although in our settings we considered this effect by using a much longer purging time compared to other works (Li et al., 2011; Li et al., 2012), the problem of higher GPC in atmospheric conditions could not be avoided. However, Shang et al., (2017), that used a purging time of 300 sec got a GPC rate of 0.39 nm/cycles for APALD deposition of TiO_2, which also does not match with the values in this research. The main reason may be due to difference in ALD cycles and experimental conditions used in this research and Shang et al., (2017), where the exposure time of

the precursors was 5 sec, the purging time was 300 sec and the cycles used was 1, 3, 8 and 13.

5.2 Effect of ALD on Water Permeability

Figure 5.1 shows the measured permeability of the 12 pristine membranes. The permeability's of the pristine membranes were between 24 – 42 L/m^2/hr/bar. This variation in the permeability values suggests that the pore sizes of the pristine membranes are not same and there is variation in the pore size. Figure 5.2 shows the permeability of the six-coated membranes, before and after ALD coating. After ALD coating, the permeability of all membranes was lower. This decrease in permeability indicates that the pore size and the porosity of the coated membranes got reduced (Shang et al., 2017), but the membranes were still permeable except M2. Of the three deposited membrane sets, (M2, M4) showed the lowest permeability, and the permeability of M2 was zero even after running the test for 1 hour. The lowest permeability of (M2 M4) meets our expectations because this set showed the highest GPC rate; this means that the reduction of pore size for this set was the highest. The GPC for M2 was the highest, and the value was also much higher compared to the values found in literature (Lei et al., 2012, Sun et al., 2012). The high GPC value of M2 indicated that the pores got completely blocked by TiO_2, which resulted in zero permeability. For the other membrane sets, the permeability reduced to 7- 15 L/m2/hr/bar. This reduction in permeability suggests that the pore sizes of the membranes were reduced, but it cannot imply that the rejection capacity improved. The effect of ALD on membrane rejection was investigated by the MWCO test.

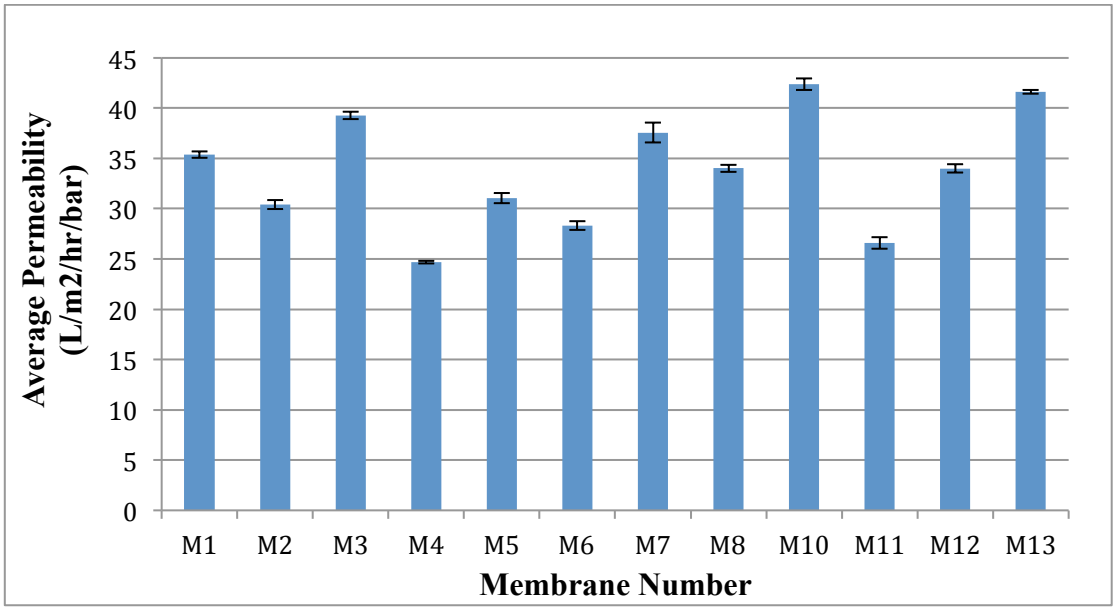

Figure 5.1: Average permeability of the pristine membranes corrected for temperature at 20^0 C (Average ± standard deviation from three measurements)

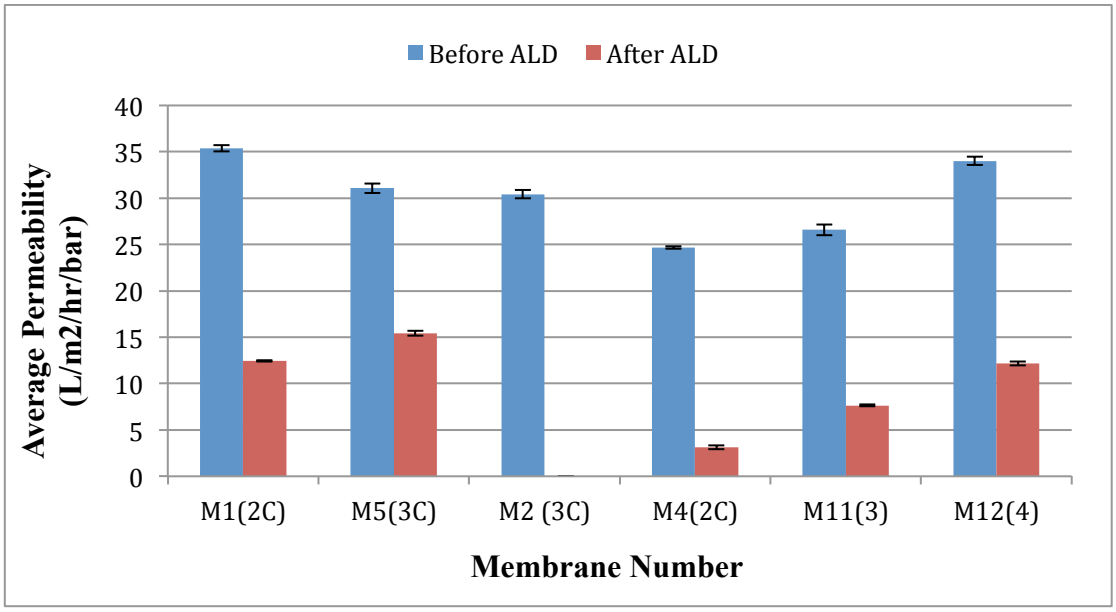

Figure 5.2: Comparison of the average permeability of the pristine and coated membranes corrected for temperature at 20^0 C (Average ± standard deviation from three measurements)

5.3 Effect of ALD on MWCO value of the membranes

The effect of ALD on the rejection performance of the membranes can be tested by the change in MWCO values of the membranes after coating. Figure 5.4

shows the MWCO of the pristine membranes. The MWCO values ranges between 3000-4000 Da except for M3, M10 and M13. The reason for the higher values of M3, M10 and M13 membranes can be due to the presence of bigger pore size in these membranes, as these 3 membranes also showed higher permeability compared to others; this allowed the larger PEG molecules to permeate. Figure 5.5 shows the comparison of the MWCO of the six coated membranes, before and after coating. After coating the MWCO for M2 was zero, which was obvious, as the membrane was not permeable anymore; however, surprisingly, membrane M4 showed higher MWCO value compared to the pristine one. This anomaly in MWCO for M4 could have been due to development of defects in the membrane, as shown in figure 5.3: the modelled rejection graph and the measured rejection curve do not match, depicting formation of defects. These defects could have resulted during the storage of membranes under ultrapure water, storage in oven after cleaning or during ALD treatment. Among the other membranes (M1, M5, M11 and M12), only M1 showed a significant MWCO decrease, although their permeability drop was similar; this is shown in Table 5.2.

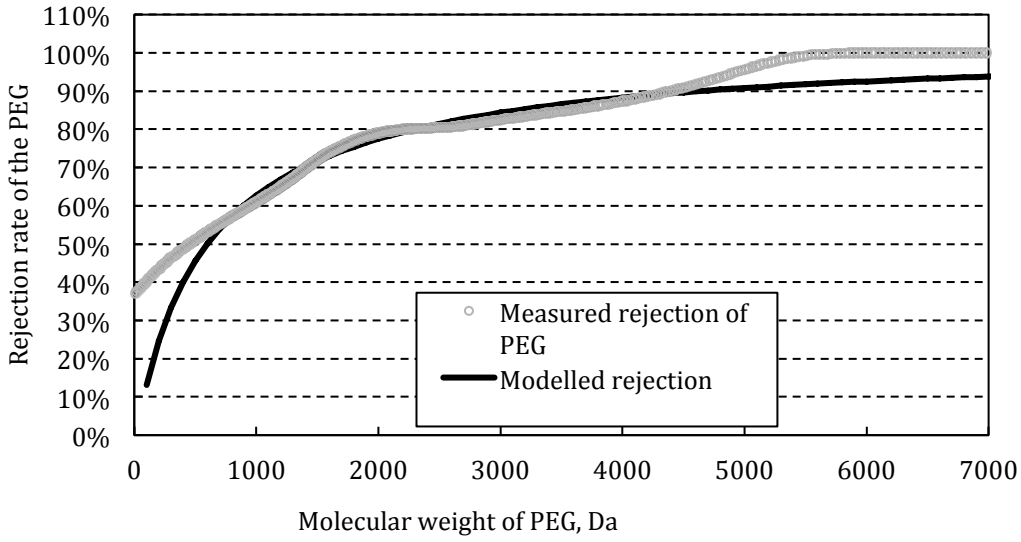

Figure 5.3: Graph for modelled and measured PEG rejection for M4 after coating

For set (M1, M5), the MWCO value of M1 after ALD dropped by 1200 Da whereas for M5 the value decreased by only 200 Da, and there no defects were observed. This high decrease in MWCO for M1 indicates that ALD caused significant reduction of pores in M1 which in turn improved the rejection capacity. Although the

GPC for both M1 and M5 was the same and both of the membranes showed similar permeability drop, they had different MWCO; the effect of ALD was thus not similar for the two membranes. This discrepancy might be due to not uniform coating in all the pores of M5: some pores did not change, and some pores were blocked. The blocked pores did not allow the permeation of liquid anymore, resulting in low permeability. These blocked pores did also not influence the pore size distribution, while the larger PEG molecules passed through the unchanged pores. M1 showed a significant change in MWCO value, but due to high GPC rate (almost 1 nm/cycle), it can be said that ALD obtained for this experimental condition was not acceptable. The size of the membrane pores was not measured directly, but equation 4.8 was applied, using the MWCO value. The calculated pore size was around 2 nm, as shown in table 5.2; therefore, with a GPC of 1 nm/cycle, it can be expected that the pores may get totally blocked after 2 or 3 cycles. However, the membranes were still permeable, showing that which explains that the deposition rate on the wafers and on the membranes was totally different.

For membrane set (M11, M12), the MWCO value decreased by 700 and 500 Da for M11 and M12 respectively; these membranes also did not show defects. Although this change in MWCO is smaller than that in M1, it was acceptably consistent with the measured GPC rate on the wafers. The MWCO values obtained for M11 and M12 indicates that the experimental conditions were favorable for proper application of ALD and the deposition helped in reducing pore size distribution. By increasing the number of cycles or by further coating, the rejection capacities of M11 and M12 could have been further improved, but it was not done in this study. M11 and M12 had a different number of cycles 4 for M12 and 3 for M11; however, M11 showed higher MWCO reduction compared to M12 because the GPC of M11 was larger.

Of the 6-coated membranes, M11 and M12 showed an acceptable improvement in rejection capacity in relation to GPC rate. This shows that ALD can be a way to fabricate tight ceramic membranes with better rejection capacity, but the great variation in the results will require further study. Studies on ALD deposition on tubular membranes having length around 10 cm have shown good deposition and significant improvement in rejection performance (Shang et al., 2017; Li, 2018). So,

with proper experimental conditions, ALD can also be done for long tubular membranes.

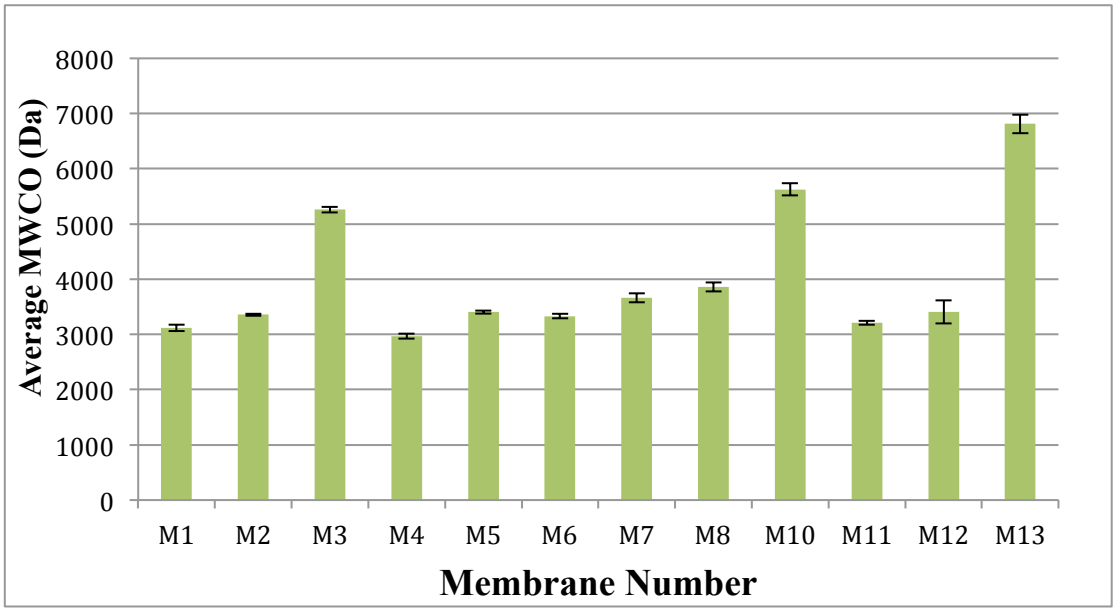

Figure 5.4: Average MWCO of the pristine membranes (Average ± standard deviation from three measurements)

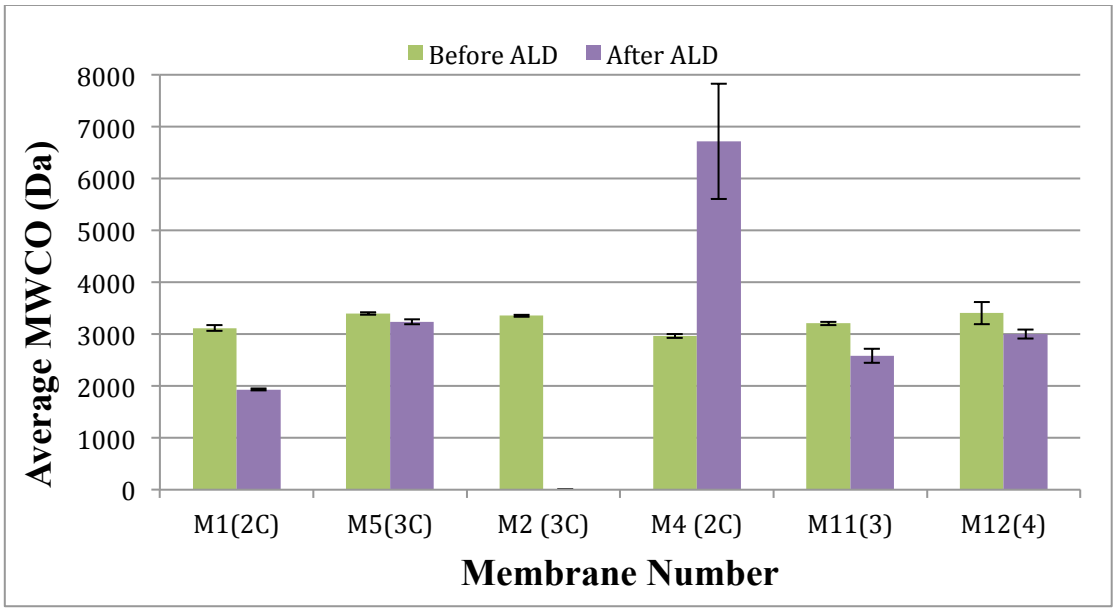

Figure 5.5: Comparison of the average MWCO of the pristine and coated membranes (Average ± standard deviation from three measurements)

Table 5.2: Change in Permeability and MWCO of M1, M5, M11 and M12 after coating

	L_p Before coating	**L_p After coating**	**MWCO Before coating**	**MWCO After coating**	**Drop in L_p**	**Drop in MWCO**	**D before coating**
M1	35.365	12.428	3100	1900	22.937	1200	2.20
M5	31.068	15.425	3400	3200	15.643	200	2.29
M11	26.578	7.637	3200	2500	18.941	700	2.23
M12	34.006	12.165	3500	3000	21.841	500	2.29

L_p = Average of the measured permeability (L/m2/hr/bar)
D = Membrane pore size calculated using Eq. 4.8 (nm)
MWCO = Average of the measured Molecular weight cut-off (Da)

6. Carman-Kozeny Model

6.1 Introduction and Equation

The Carman-Kozeny equation shows a relation between the pressure drop for laminar flow in a packed bed of solids. Josef Kozeny originally designed the equation back in 1927, when he developed a model containing a number of parallel capillary tubes of equal length and diameter to describe the pressure drop for laminar flow in a packed bed of solids (Kruczek, 2014; McCabe et al., 1993). This equation was then combined with Hagen-Poiseulille law to determine the flow of fluid through the pores in a membrane, considering that the pores are not cylindrical and straight (Kruczek, 2014). The modified Carman-Kozeny equation is shown in Eq. 6.1 (Kruzek, 2014), and this relation is used in our study to simulate the flux through the membranes assuming that the pores are interstices between close-packed spheres (Seader et al., 1998). The permeabilities obtained by this model are then compared with the measured permeability values.

$$J = \frac{\varepsilon^3 \, \Delta P}{2 \, (1-\varepsilon)^2 \, \tau \, a_v^2 \, \mu \, l} \qquad \text{Eq. 6.1}$$

where,

J = flux through membrane, $m^3/(m^2 \cdot s)$
ρ = density of the fluid, kg/m^3
ε = porosity of membrane, -
ΔP = transmembrane pressure, pa
τ = tortuosity factor, -
a_v = specific surface area, $1/m$
μ = viscosity of the fluid, $pa \cdot s$
l = layer thickness, m

6.2 Assumptions

The following assumptions were made while estimating the water permeability using Carman-Kozeny equation:

a) The feed water into the membrane was at room temperature (20^0C) and at atmospheric pressure (101 325 Pa); therefore, the dynamic viscosity (μ) was 0.001 Pa s.

b) The hydraulic diameter of the membrane pores (D) was assumed to be close to the average pore size and can be estimated by using Eq. 6.2 (Seader et al., 1998)

$$D = 0.065\ (MWCO)^{0.438} \qquad \text{Eq. 6.2}$$

c) The specific surface area is related to the porosity and hydraulic diameter of the membrane pores as shown in Eq. 6.3 (Seader et al., 1998)

$$a_v = \frac{4\varepsilon}{D\ (1-\varepsilon)} \qquad \text{Eq. 6.3}$$

d) The tortuosity of the membranes was taken as 2.08 (Li, 2018)

e) The thickness of the separation layer (*l*) was taken as 350 nm.

f) The porosity of all pristine membranes was back calculated using Eq. 6.1 and the average value (0.40) was taken to simulate the model.

g) Eq. 6.4 was used to determine the porosity of the membranes after ALD where the shape of the pores were assumed to be spherical and the number of pores after coating (n) were assumed to be constant, making the change in porosity only related to the change in pore size.

$$\varepsilon_i = \frac{void\ volume}{total\ volume} = \frac{n\ \frac{\pi\ D_i^3}{6}}{V_{total}}$$

$$\rightarrow \frac{\varepsilon_{before}}{\varepsilon_{after}} = \left(\frac{D_{before}}{D_{after}}\right)^3 \qquad \text{Eq. 6.4}$$

h) The pore size and thickness of the top layer (separation/filtration layer) were not measured by means of Brunauer-Emmett-Teller theory (Shang et al., 2017), scanning electron microscope image measurement (Li, 2018), and also the coating depth by EDX measurement (Li et al., 2018); therefore, it was assumed that the coating takes place in the entire filtration layer. As a result, a Two-Layer model concept as used by Li (2018) was not taken into consideration in this report.

6.3 Procedure

Figure 6.1 shows the 2 methods used in determining the pore size of the membranes after coating and subsequently the permeability's. In Method 1, the measured MWCO was used to calculate the pore size of the membranes before and after coating using Eq. 6.2, and then Eq. 6.4 was used to calculate the porosity of the membranes after coating. With the new porosity and pore size the model permeability was then calculated by Eq. 6.1. For Method 2, the pore sizes of the pristine membranes were calculated by Eq. 6.2, and the pore size of the membranes after coating was calculated based on the GPC measured on the wafer. After that, the porosity and permeability were calculated as in Method 1.

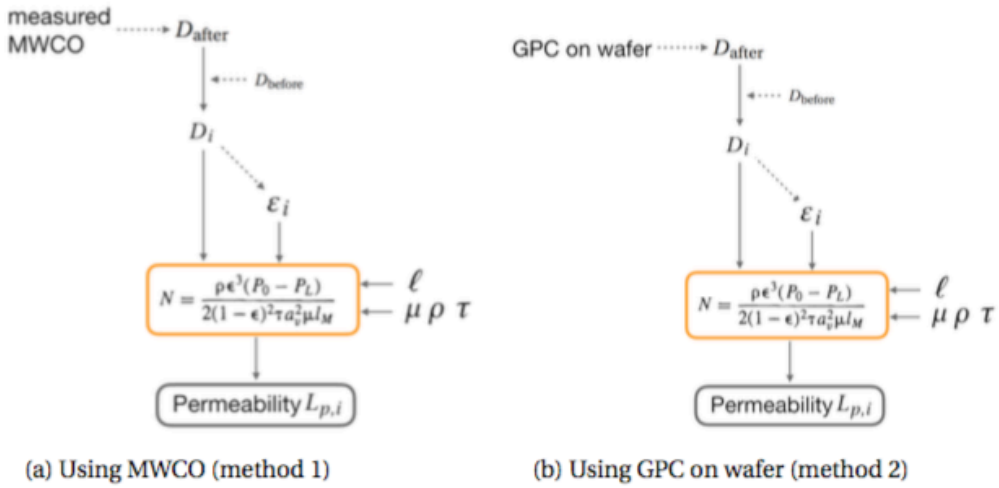

Figure 6.1: Schematic view of Carman-Kozeny Model procedure (Li, 2018)

6.4 Model Results

The model results for permeability's, before and after coating, using Method 1 and Method 2 are shown in Table 6.1 and Table 6.2 respectively. In both the methods, M2 and M4 membrane were not used. For M2 the permeability and MWCO value was zero after coating and the GPC was also high (making the pore size after coating negative), so the model cannot be justified for any methods (MWCO method or GPC method). Similarly, for M4 the MWCO after coating was high plus the GPC was also high, making the model results unjustified.

For Method 1, all the membranes, with exception of M1, showed deviated permeability values from the measured one. This deviation is expected, as these membranes didn't show much change in MWCO values although there was decrease in permeability. For M1 the model result matches with the measured value indicating that the assumptions for porosity, tortuosity, estimated pore size and filtration layer thickness works well.

For Method 2, the modelled porosity of M1 and M5 was zero, due to the fact that the GPC on wafers corresponding to these membranes were very high, which overestimated the pore size to zero. This validates the fact that the GPC on the membrane pores were not same as on wafers since the membranes were still permeable. For M11 and M12, the model results fit properly to the measured result, indicating that the GPC on wafer was same as that in the pores. Also, the validation of model results for M11 and M12 indicates that the initial assumptions were appropriate.

Table 6.1: Permeability values of the Carman-Kozeny model before and after coating by using Method 1 (MWCO)

Membrane Number	**Before Coating**			**After Coating**		
	ε^{*1}	L_p	$L^*_{p,model}$	ε^{*2}	L_p	$L^*_{p,model}$
M1	0.40	35.36	33.61	0.22	12.43	12.24
M5	0.40	31.07	32.10	0.37	3.12	32.24
M11	0.40	26.58	34.54	0.30	7.64	21.46
M12	0.40	34.00	36.42	0.34	12.16	27.8

* = estimated using Carman-Kozeny equation
*1 = assumed starting porosity
*2 = estimated porosity using Eq. 6.4
L_p = measured permeability in the filtration test (L/m2/hr/bar)

Table 6.2: Permeability values of the Carman-Kozeny model before and after coating by using Method 2 (GPC on wafer)

Membrane Number	Before Coating			After Coating		
	ε^{*1}	L_p	$L^*_{p,model}$	ε^{*2}	L_p	$L^*_{p,model}$
M1	0.40	35.36	33.61	0.00	12.43	0
M5	0.40	31.07	32.10	0.00	3.12	0
M11	0.40	26.58	34.54	0.10	7.64	5.67
M12	0.40	34.00	36.42	0.22	12.16	13.65

* = estimated using Carman-Kozeny equation
*1 = assumed starting porosity
*2 = estimated porosity using Eq. 6.4
L_p = measured permeability in the filtration test (L/m2/hr/bar)

6.5 Model Sensitivity

In order to check the influence of membrane pore size and membrane porosity, model sensitivity analysis was performed using different membrane porosity. Figure 6.2 shows the change in permeability with change in pore size at different porosity. When the pore size increases, the difference in permeability values at different porosity also increases. At pore size 2 nm, which is the estimated pore size of our membranes, the difference in permeability value between porosity of 0.50 to 0.30 is around 13 L/m2/hr/bar. However, when the porosity is kept fixed, the methods used in determination of pore size can also make differences in permeability values. As shown before, using Method 1 only membrane M1 matches the model permeability value, whereas for Method 2 only M11 and M12 validates the model.

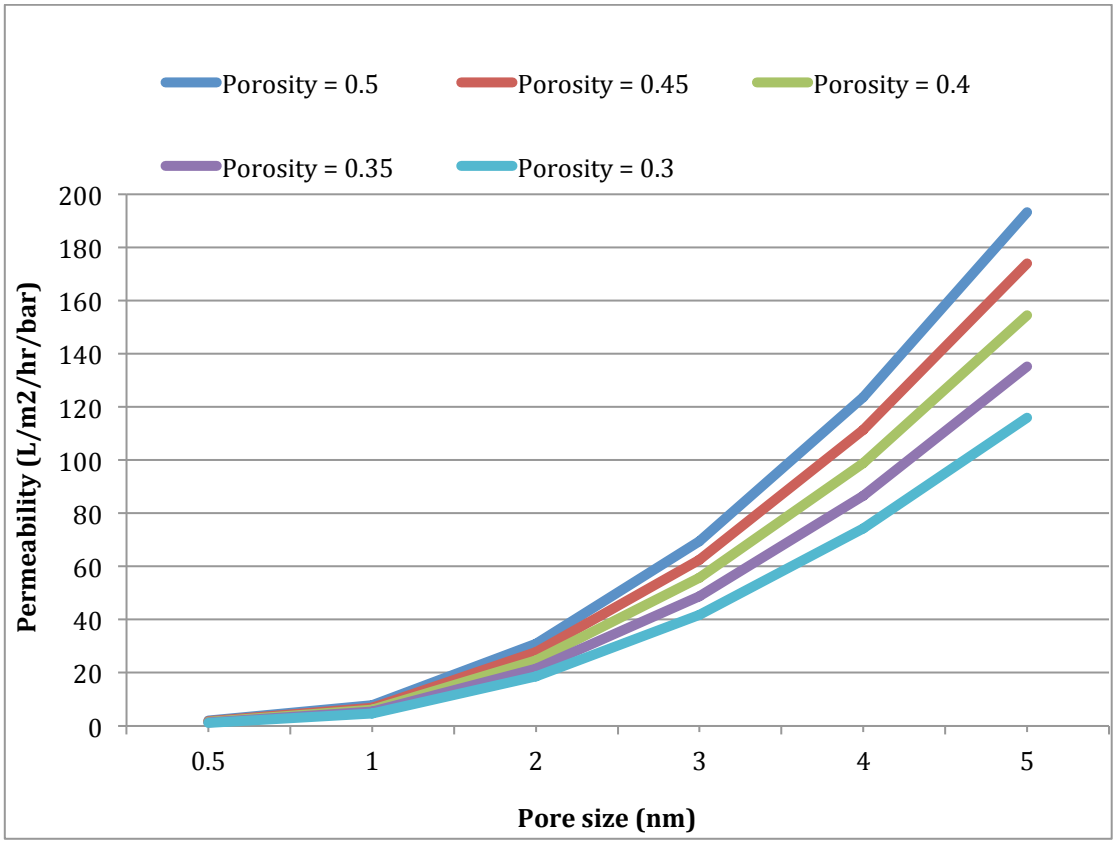

Figure 6.2: Sensitivity analysis of Carman-Kozeny model

6.6 Limitations of the model

The Carman-Kozeny model can be used to predict the permeability of ceramic membranes after ALD coating, but there are a few limitations associated with this model. First, for determining the pore size and permeability of the membranes Eq. 6.1 is used, which is very uncertain based on membrane surface porosity and tortuosity. Second, the structure related parameters used in the model (such as pore size, pore size distribution, top layer thickness and porosity) were not measured directly, but they were either back calculated based on filtration results or assumed. Therefore, without proper measurements, the assumptions and calculated values may not be correct to fit the model. Third, this model is based on closed-packed-pattern; however, the ceramic particles are not well packed, which may result in difference between model and measured results. Fourth, the model was developed as one layer model, considering the fact that the coating took place in the entire filtration layer. In reality, the coating may take place up to a certain depth in the filtration layer based on effective coating depth. Even though the effective coating depth is measured, a clear

boundary doesn't exist and the thickness of the deposited films may decrease gradually from there. So, we can conclude that there is always some uncertainty associated with the calculated permeability through this model.

7. Conclusion and Recommendations

This research was done to study the effect of ALD on tubular ceramic membranes in order to improve the membrane rejection performance. Tubular membranes having length of 0.5 m and internal diameter 0.008 m were used as substrate membranes, and APALD was used to deposit TiO_2 on the membranes. The effect of ALD was determined with membrane filtration experiments, consisting of ultrapure water permeability and MWCO (based on PEG rejection). The pristine membranes showed permeability and MWCO around 30 L/m2/hr/bar and 3000 Da respectively. The growth rate of TiO_2 on the ceramic membranes was measured indirectly on silicon wafers through ellipsometry, but the GPC was different for different membranes. After ALD coating, the membranes showed decrease in water permeability compared to the original substrate membranes, indicating decrease in porosity, although the pores of one membrane (M2) became totally blocked due to high amount of deposition. Considering the rejection performance in relation to the measured GPC of the deposited layers, only two coated membranes (M11 and M12) showed acceptable improvement of rejection. One membrane, M1, showed a high rejection improvement; however, the results is not considered acceptable because the GPC rate was much higher than expected and did not match the MWCO measurement. Another membrane, M5, did not show change in MWCO, although the GPC measured was same as in M1. These discrepancies suggest that the ALD deposition on the membranes was not same as obtained in the wafers, and also that the deposition was not uniform in all pores: some pores were blocked and some pores did not change their size..

The Carman-Kozeny model was used to numerically predict the water permeability of the coated membranes. The model was applied using two methods (MWCO and GPC on wafer) and the results were compared with the measured values. Based on the method used, the model fits the measured data of some of the membranes, showing that the model can be used to predict the change in permeability with change in membrane properties, even though there are some limitations associated with the model.

Although, in this work, the results on the influence of ALD on the membrane rejection performance was contradictory. However, the GPC and MWCO results obtained for the ALD settings used to coat M11 and M12 were satisfactory, and it can be tested if the rejection performance of these two membranes could be improved by increasing the number of deposition cycles. Also, from the experimental results it can be concluded that a long purging time plays an important role in ALD coating for ceramic membranes. ALD can still be a convenient technique to fabricate tight ceramic membranes having improved rejection performance without much loss in permeability; however, as only 2 out of 6 coated membranes showed acceptable results, a better-controlled deposition is necessary for tubular ceramic membranes of this length.

In a further study, we recommend to apply new ALD layers to the membranes that showed acceptable results, M11 and M22 using the same experimental conditions. Also, it will be necessary to choose experimental conditions that guarantee uniform deposition of TiO_2 on all the membrane pores and control of pore size for 0.5 m long tubular membranes. We also recommend to perform scanning electron microscope (SEM), energy dispersive X-ray spectroscopy (EDX) and Brunauer Emmett Teller (BET) analysis in order to determine the pore structure, pore size distribution, effective coating depth and the thickness of the various layers. These analyses will help to better understand the effect of ALD coating and find the reasons for the discrepancies found in this research.

Appendix:

Table A: Average permeability corrected for temperature at 20^0 C and average MWCO of the pristine membranes
(Average ± standard deviation from three measurements)

Membrane Number	Average Permeability of the pristine membranes ($L/m^2/hr/bar$)	Average MWCO of the pristine membranes (Da)
M1	35.365 ± 0.328	3100 ± 100
M2	30.405 ± 0.438	3300 ± 100
M3	39.290 ± 0.379	5200 ± 100
M4	24.677 ± 0.136	3000 ± 100
M5	31.068 ± 0.518	3400 ± 100
M6	28.335 ± 0.444	3300 ± 100
M7	37.558 ± 0.991	3600 ± 100
M8	34.011 ± 0.349	3800 ± 100
M10	42.368 ± 0.561	5600 ± 100
M11	26.578 ± 0.580	3200 ± 100
M12	34.006 ± 0.431	3500 ± 100
M13	41.609 ± 0.172	6900 ± 100

Table B: Average permeability corrected for temperature at 20^0 C and average MWCO of the coated membranes
(Average ± standard deviation from three measurements)

Membrane Number	Average Permeability of the pristine membranes ($L/m^2/hr/bar$)	Average MWCO of the pristine membranes (Da)
M1	12.428 ± 0.057	1900 ± 100
M2	0	0
M4	3.116 ± 0.192	7000 ± 100
M5	15.425 ± 0.257	3200 ± 100
M11	7.637 ± 0.084	2500 ± 100
M12	12.165 ± 0.208	3000 ± 100

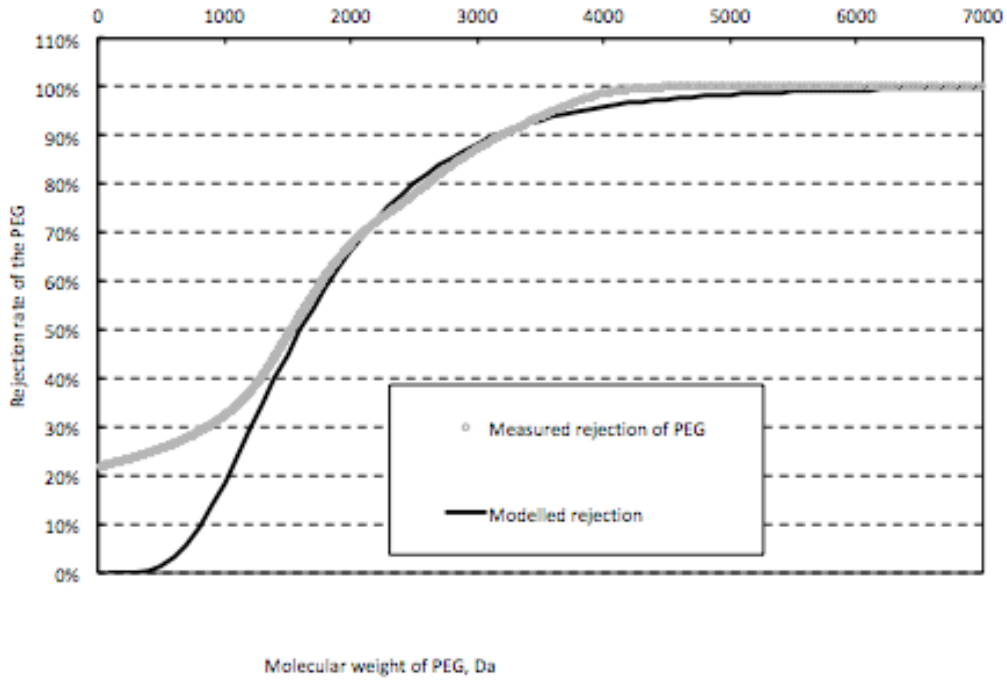

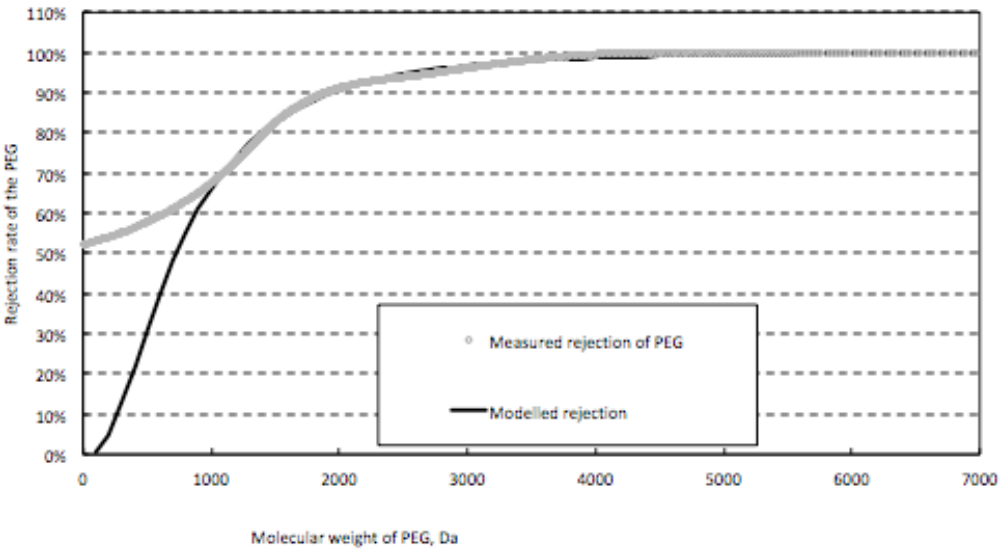

Figure A: Graph for modelled and measured PEG rejection for M1 before (up) and after (down) coating

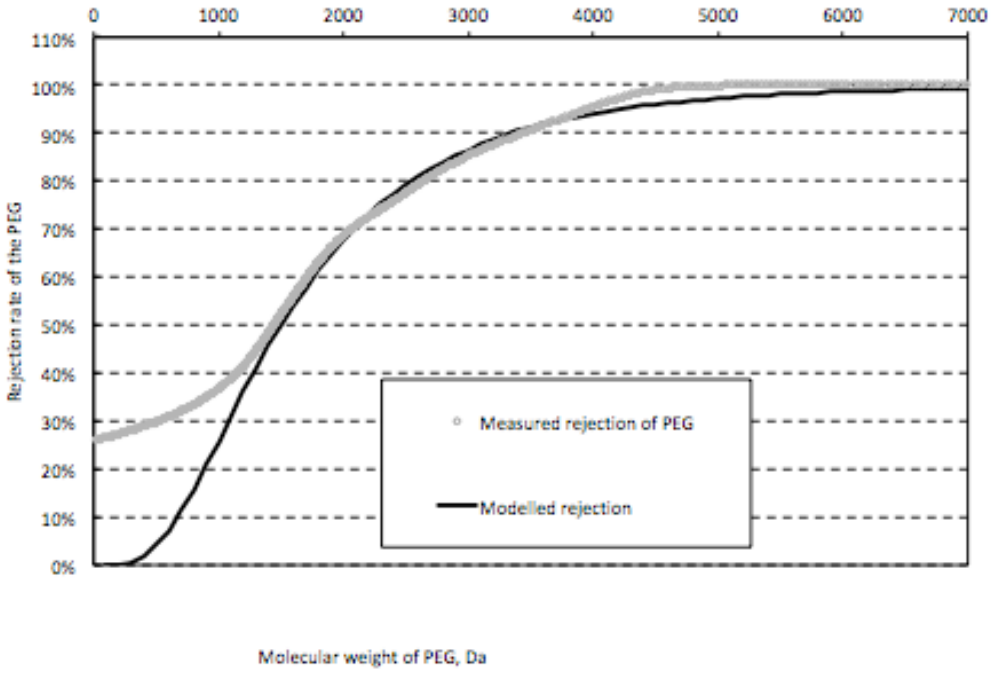

Figure B: Graph for modelled and measured PEG rejection for M2 before coating

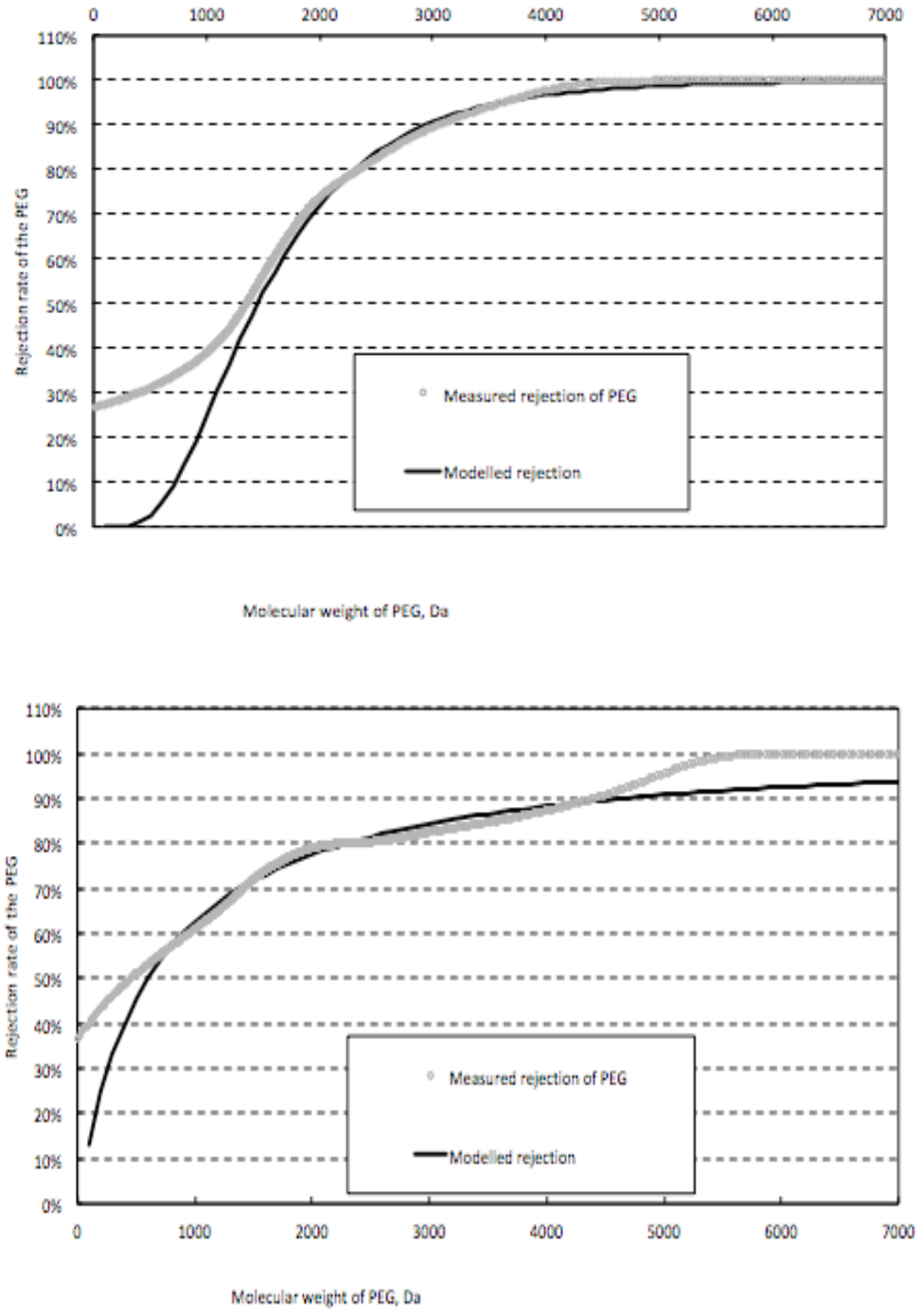

Figure C: Graph for modelled and measured PEG rejection for M4 before (up) and after (down) coating

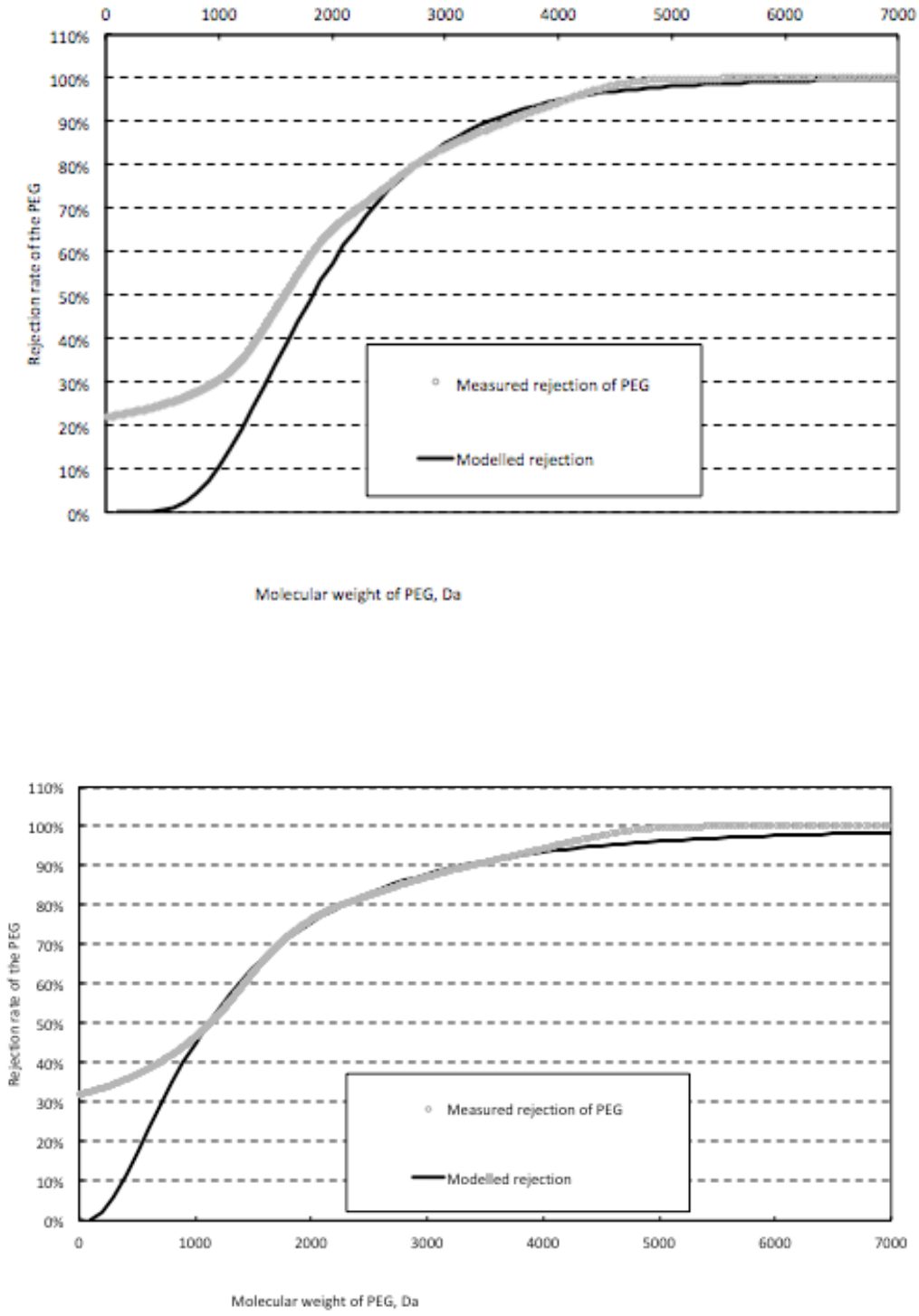

Figure D: Graph for modelled and measured PEG rejection for M5 before (up) and after (down) coating

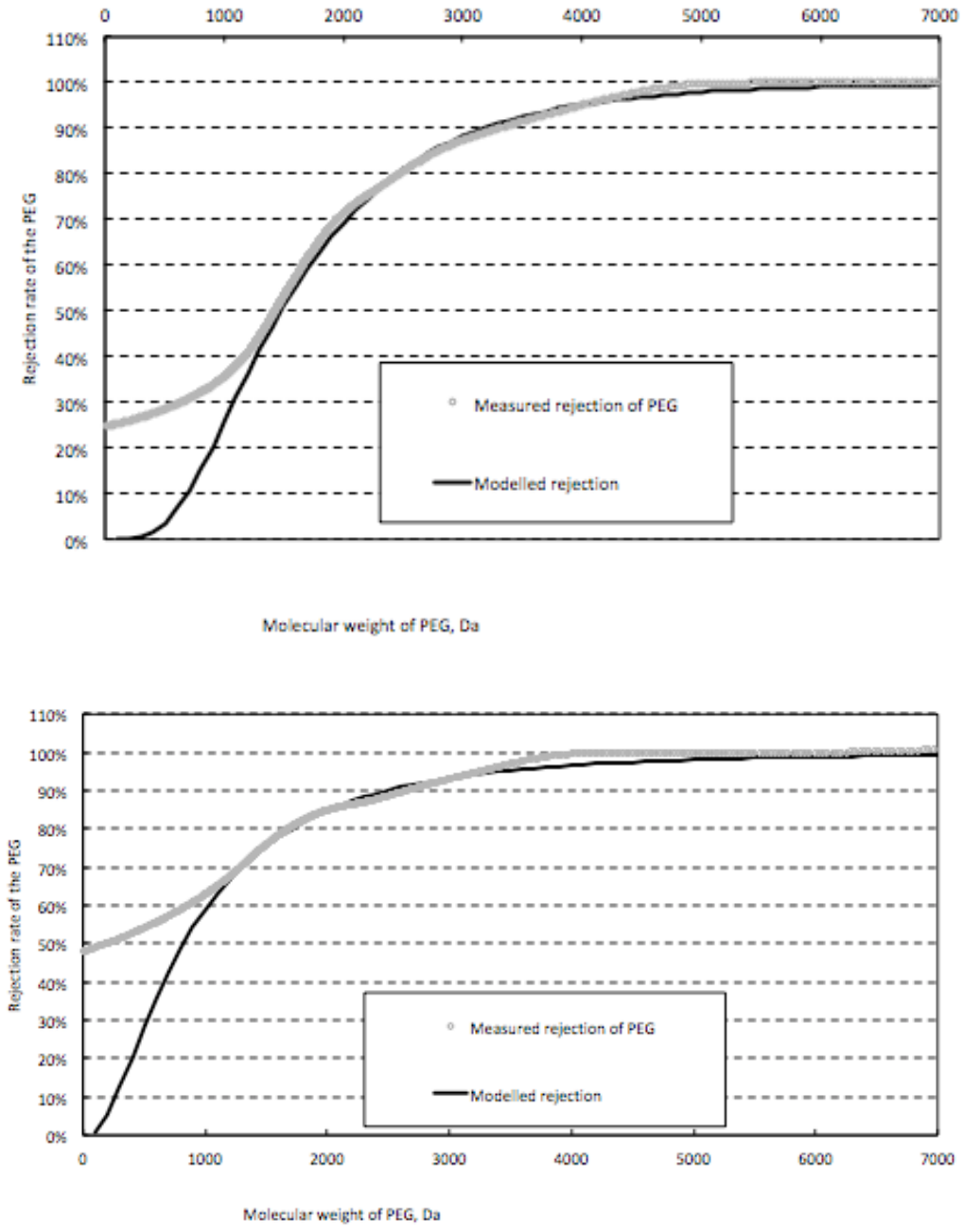

Figure E: Graph for modelled and measured PEG rejection for M11 before (up) and after (down) coating

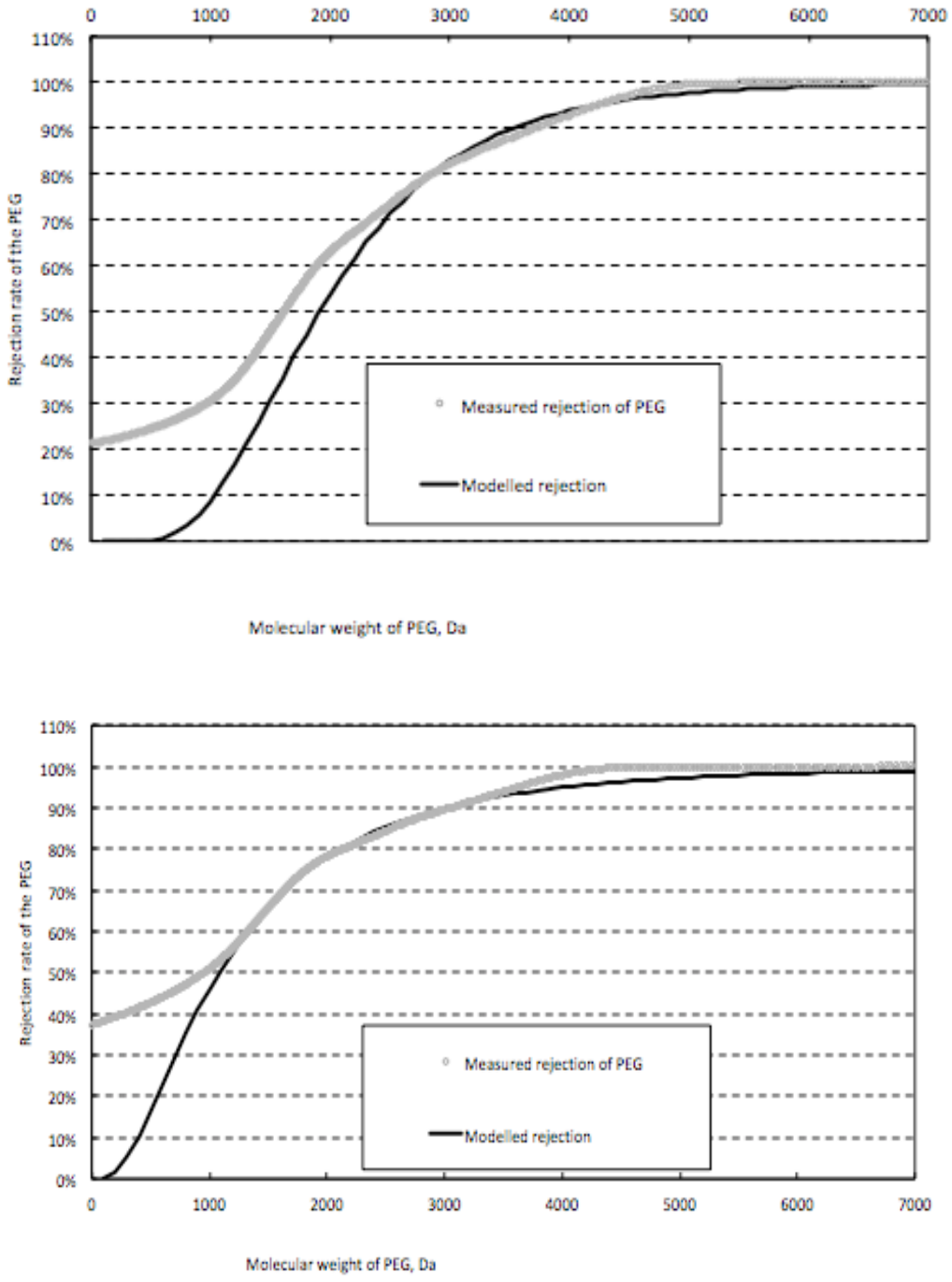

Figure F: Graph for modelled and measured PEG rejection for M12 before (up) and after (down) coating

References:

1) Abdulagatov, A. I., Hall, R. A., Sutherland, J. L., Lee, B. H., Cavanagh, A. S., & George, S. M. (2012). Molecular layer deposition of titanicone films using TiCl4 and ethylene glycol or glycerol: growth and properties. Chemistry of Materials, 24(15), 2854-2863.

2) Alessandri, I., Zucca, M., Ferroni, M., Bontempi, E., & Depero, L. E. (2009). Tailoring the pore size and architecture of CeO2/TiO2 core/shell inverse opals by atomic layer deposition. Small, 5(3), 336-340.

3) Alf, M. E., Asatekin, A., Barr, M. C., Baxamusa, S. H., Chelawat, H., Ozaydin‐Ince, G., ... & Vaddiraju, S. (2010). Chemical vapor deposition of conformal, functional, and responsive polymer films. Advanced Materials, 22(18), 1993-2027.

4) Babaluo, A. A., Kokabi, M., Manteghian, M., & Sarraf-Mamoory, R. (2004). A modified model for alumina membranes formed by gel-casting followed by dip-coating. Journal of the European Ceramic Society, 24(15-16), 3779-3787.

5) Benfer, S., Popp, U., Richter, H., Siewert, C., & Tomandl, G. (2001). Development and characterization of ceramic nanofiltration membranes. Separation and purification technology, 22, 231-237.

6) Bhave, R. (2012). Inorganic Membranes Synthesis, Characteristics and Applications: Synthesis, characteristics, and applications. Springer Science & Business Media.

7) Bonekamp, B. C. (1996). Preparation of asymmetric ceramic membrane supports by dip-coating. In Membrane Science and Technology (Vol. 4, pp. 141-225). Elsevier.

8) Boryło, P., Matus, K., Lukaszkowicz, K., Kubacki, J., Balin, K., Basiaga, M., ... & Mikuła, J. (2018). The influence of atomic layer deposition process temperature on ZnO thin film structure. Applied Surface Science.

9) Burggraaf, A. J., & Cot, L. (2009). Fundamentals of Inorganic Membrane Science and Technology, 1996.

10) Calvert, P. D., Lalanandham, R. R., Parish, M. V., Fox, J., Lee, H., Pober, R. L., ... & Bowen, H. K. (1986). Dispersion of ceramic particles in organic liquids. MRS Online Proceedings Library Archive, 73.

11) Chang, Q., Zhou, J. E., Wang, Y., Liang, J., Zhang, X., Cerneaux, S., ... & Dong, Y. (2014). Application of ceramic microfiltration membrane modified by nano-TiO2 coating in separation of a stable oil-in-water emulsion. Journal of Membrane Science, 456, 128-133.

12) Chen, H., Jia, X., Wei, M., & Wang, Y. (2017). Ceramic tubular nanofiltration membranes with tunable performances by atomic layer deposition and calcination. Journal of Membrane Science , 528 , 95-102.

13) Chen, H., Wu, S., Jia, X., Xiong, S., & Wang, Y. (2018). Atomic layer deposition fabricating of ceramic nanofiltration membranes for efficient separation of dyes from water. AIChE Journal.

14) Chon, K., & Cho, J. (2016). Fouling behavior of dissolved organic matter in nanofiltration membranes from a pilot-scale drinking water treatment plant: An autopsy study. Chemical Engineering Journal, 295, 268-277.

15) Combe, C., Guizard, C., Aimar, P., & Sanchez, V. (1997). Experimental determination of four characteristics used to predict the retention of a ceramic nanofiltration membrane. Journal of Membrane Science, 129(2), 147-160.

16) Condom, S., Larbot, A., Younssi, S. A., & Persin, M. (2004). Use of ultra-and nanofiltration ceramic membranes for desalination. Desalination, 168, 207-213.

17) da Silva Biron, D., dos Santos, V., & Zeni, M. (2018). Applications of Ceramic Membranes. In Ceramic Membranes Applied in Separation Processes (pp. 67-80). Springer, Cham.

18) Das, N., & Maiti, H. S. (2009). Ceramic membrane by tape casting and sol–gel coating for microfiltration and ultrafiltration application. Journal of Physics and Chemistry of Solids, 70(11), 1395-1400.

19) Dasgupta, J., Mondal, D., Chakraborty, S., Sikder, J., Curcio, S., & Arafat, H. A. (2015). Nanofiltration based water reclamation from tannery effluent following coagulation pretreatment. Ecotoxicology and environmental safety, 121, 22-30.

20) Drioli, E., Giorno, L., & Fontananova, E. (Eds.). (2017). Comprehensive membrane science and engineering. Elsevier.

21) George, S. M. (2009). Atomic layer deposition: an overview. Chemical reviews, 110(1), 111-131.

22) Gitis, V., & Rothenberg, G. (2016). Ceramic membranes: new opportunities and practical applications. John Wiley & Sons.

23) Grigoras, K., Airaksinen, V. M., & Franssila, S. (2009). Coating of nanoporous membranes: atomic layer deposition versus sputtering. Journal of nanoscience and nanotechnology, 9(6), 3763-3770.

24) Gu, H., Rahardianto, A., Gao, L. X., Christofides, P. D., & Cohen, Y. (2016). Ultrafiltration with self-generated RO concentrate pulse backwash in a novel integrated seawater desalination UF-RO system. Journal of Membrane Science, 520, 111-119.

25) Guizard, C., Ayral, A., & Julbe, A. (2001). Present status and new developments of ceramic nanofiltration membranes. In Proceedings of the 3rd Nanofiltration and Application Workshop, Lappeenrata, Finland.

26) Hsieh, H. P. (1996). Inorganic membranes for separation and reaction (Vol. 3). Elsevier.

27) Kayvani Fard, A., McKay, G., Buekenhoudt, A., Al Sulaiti, H., Motmans, F., Khraisheh, M., & Atieh, M. (2018). Inorganic membranes: Preparation and application for water treatment and desalination. Materials, 11(1), 74.

28) Kemell, M., Ritala, M., Leskelä, M., Groenen, R., & Lindfors, S. (2008). Coating of highly porous fiber matrices by atomic layer deposition. Chemical Vapor Deposition, 14(11‐12), 347-352.

29) Koutsonikolas, D. E., Kaldis, S. P., & Pantoleontos, G. T. (2017). Preparation of Silica Membranes by Atomic Layer Deposition. In Current Trends and Future Developments on (Bio-) Membranes (pp. 45-62).

30) Kruczek, B. (2014). Carman–Kozeny Equation. In Encyclopedia of Membranes (pp. 1-3). Springer Berlin Heidelberg.

31) Labropoulos, A. I., Athanasekou, C. P., Kakizis, N. K., Sapalidis, A. A., Pilatos, G. I., Romanos, G. E., & Kanellopoulos, N. K. (2014). Experimental investigation of the transport mechanism of several gases during the CVD post-treatment of nanoporous membranes. Chemical Engineering Journal, 255, 377-393.

32) Laitinen, N. (2001). Development of a ceramic membrane filtration equipment and its applicability for different wastewaters. Acta Universitatis Lappeenrantaensis.

33) Larbot, A. (1996). Ceramic processing techniques of support systems for membranes synthesis. In Membrane Science and Technology (Vol. 4, pp. 119-139). Elsevier.

34) Lee, M., Wu, Z., & Li, K. (2015). Advances in ceramic membranes for water treatment. In Advances in Membrane Technologies for Water Treatment (pp. 43-82).

35) Lei, Y., Liu, B., Lu, J., Lobo-Lapidus, R. J., Wu, T., Feng, H., ... & Miller, J. T. (2012). Synthesis of Pt–Pd core–shell nanostructures by atomic layer deposition: application in propane oxidative dehydrogenation to propylene. Chemistry of Materials, 24(18), 3525-3533.

36) Lei, Y., Lu, J., Zhao, H., Liu, B., Low, K. B., Wu, T., ... & Elam, J. W. (2013). Resolving precursor deligation, surface species evolution, and nanoparticle

nucleation during palladium atomic layer deposition. The Journal of Physical Chemistry C, 117(21), 11141-11148.

37) Li, J. (2018). Plasma-enhanced Atomic Layer Deposition for Synthesis of ceramic Tight UF membrane. Master Thesis Report.

38) Li, K. (2007). Ceramic membranes for separation and reaction. John Wiley & Sons.

39) Li, F., Li, L., Liao, X., & Wang, Y. (2011). Precise pore size tuning and surface modifications of polymeric membranes using the atomic layer deposition technique. Journal of membrane science, 385, 1-9.

40) Li, F., Yang, Y., Fan, Y., Xing, W., & Wang, Y. (2012). Modification of ceramic membranes for pore structure tailoring: The atomic layer deposition route. Journal of membrane science, 397, 17-23.

41) Liu, D. M. (Ed.). (1996). Porous ceramic materials: fabrication, characterization, applications. Trans Tech Publ.

42) Losic, D., Triani, G., Evans, P. J., Atanacio, A., Mitchell, J. G., & Voelcker, N. H. (2006). Controlled pore structure modification of diatoms by atomic layer deposition of TiO 2. Journal of Materials Chemistry, 16(41), 4029-4034.

43) Makhlouf, A. S. H. (2011). Current and advanced coating technologies for industrial applications. In Nanocoatings and Ultra-Thin Films (pp. 3-23).

44) Malm, J., Sahramo, E., Perälä, J., Sajavaara, T., & Karppinen, M. (2011). Low-temperature atomic layer deposition of ZnO thin films: Control of crystallinity and orientation. Thin Solid Films, 519(16), 5319-5322.

45) Marichy, C., Bechelany, M., & Pinna, N. (2012). Atomic layer deposition of nanostructured materials for energy and environmental applications. Advanced Materials, 24(8), 1017-1032.

46) McCabe, W. L., Smith, J. C., & Harriott, P. (1993). Unit operations of chemical engineering (Vol. 1130). New York: McGraw-hill.

47) Narayan, R. J., Adiga, S. P., Pellin, M. J., Curtiss, L. A., Stafslien, S., Chisholm, B., ... & Elam, J. W. (2010). Atomic layer deposition of nanoporous biomaterials. Materials Today, 13(3), 60-64.

48) Nevalainen, K., Isomäki, N., Honkanen, M., Suihkonen, R., McNally, T., Harkin‐Jones, E., ... & Järvelä, P. (2012). Melt‐compounded nanocomposites of titanium dioxide atomic‐layer‐deposition‐coated polyamide and polystyrene powders. Polymers for Advanced Technologies, 23(3), 357-366.

49) Popat, K. C., Mor, G., Grimes, C., & Desai, T. A. (2004). Poly (ethylene glycol) grafted nanoporous alumina membranes. Journal of Membrane Science, 243(1-2), 97-106.

50) Puurunen, R. L. (2005). Surface chemistry of atomic layer deposition: A case study for the trimethylaluminum/water process. Journal of applied physics, 97(12), 9.

51) Seader, J. D., Henley, E. J., & Roper, D. K. (1998). Separation process principles.

52) Sengupta, A., & Sirkar, K. K. (1995). Analysis and design of membrane permeators for gas separation. In Membrane Science and Technology (Vol. 2, pp. 499-552). Elsevier.

53) Shang, R., Goulas, A., Tang, C. Y., de Frias Serra, X., Rietveld, L. C., & Heijman, S. G. (2017). Atmospheric pressure atomic layer deposition for tight ceramic nanofiltration membranes: Synthesis and application in water purification. Journal of Membrane Science, 528, 163-170.

54) Silva, L. L., Vasconcelos, D. C., Nunes, E. H., Caldeira, L., Costa, V. C., Musse, A. P., ... & Vasconcelos, W. L. (2012). Processing, structural characterization and performance of alumina supports used in ceramic membranes. Ceramics International, 38(3), 1943-1949.

55) Skluzacek, J. M., Tejedor, M. I., & Anderson, M. A. (2007). NaCl rejection by an inorganic nanofiltration membrane in relation to its central pore potential. Journal of membrane science, 289(1-2), 32-39.

56) Sondhi, R., Bhave, R., & Jung, G. (2003). Applications and benefits of ceramic membranes. Membrane Technology, 2003(11), 5-8.

57) Song, Z., Fathizadeh, M., Huang, Y., Chu, K. H., Yoon, Y., Wang, L., ... & Yu, M. (2016). TiO 2 nanofiltration membranes prepared by molecular layer deposition for water purification. Journal of Membrane Science, 510, 72-78.

58) Spillman, R. (1995). Economics of gas separation membrane processes. In Membrane Science and Technology (Vol. 2, pp. 589-667). Elsevier.

59) Sun, X., Xie, M., Wang, G., Sun, H., Cavanagh, A. S., Travis, J. J., ... & Lian, J. (2012). Atomic layer deposition of TiO2 on graphene for supercapacitors. Journal of the Electrochemical Society, 159(4), A364-A369.

60) Triani, G., Evans, P., Attard, D., Prince, K., Bartlett, J., Tan, S. and Burford, R. (2006). Nanostructured TiO2 membranes by atomic layer deposition. Journal of Materials Chemistry, 16(14), p.1355.

61) TU Delft, Micro- and Ultrafiltration. Accessed on 15/12/18. Available at: https://ocw.tudelft.nl/wp-content/uploads/Micro-and-ultrafiltration-1.pdf

62) Ulbricht, M. (2006). Advanced functional polymer membranes. Polymer, 47(7), 2217-2262.

63) Wang, Q., Wang, X., Wang, Z., Huang, J., & Wang, Y. (2013). PVDF membranes with simultaneously enhanced permeability and selectivity by breaking the tradeoff effect via atomic layer deposition of TiO2. Journal of membrane science, 442, 57-64.

64) Wenten, I. G. (2002). Recent development in membrane science and its industrial applications. J Sci Technol Membrane Sci Technol, 24(Suppl), 1010-1024.

65) Williams, M. (2014). What percent of Earth is water. Universe Today, 2014-2016.

66) Xi, Z. Y., Xu, Y. Y., Zhu, L. P., & Zhu, B. K. (2009). Modification of polytetrafluoroethylene porous membranes by electron beam initiated surface grafting of binary monomers. Journal of Membrane Science, 339(1-2), 33-38.

67) Xin, X., Lü, Z., Zhu, Q., Huang, X., & Su, W. (2007). Fabrication of dense YSZ electrolyte membranes by a modified dry-pressing using nanocrystalline powders. Journal of Materials Chemistry, 17(16), 1627-1630.

68) Yacou, C., Wang, D., Motuzas, J., Zhang, X., Smart, S., & Diniz da Costa, J. C. (2013). Thin‐film ceramic membranes. Encyclopedia of Membrane Science and Technology, 1-36.